The role of the Rankine-Hugoniot relations in staggered finite difference schemes for the shallow water equations

Marcel Zijlema

Delft University of Technology, Department of Hydraulic Engineering, P.O. Box 5048, 2600 GA Delft, The Netherlands

Abstract

The purpose of this work is to point out the relevance of the Rankine-Hugoniot jump relations regarding the numerical solution of the inviscid shallow water equations. To arrive at physically relevant solutions in rapidly varied flow, it is of crucial importance that continuity of mass flux and momentum flux across a steady discontinuity is fulfilled at the discrete level. By adopting this viewpoint, finite difference schemes can be studied that may be well suited to solve shallow water flow problems involving discontinuities, while they are not based on a characteristic decomposition of the governed hyperbolic equations. Three schemes on staggered grids with either the water level or the water depth at the cell centre and the flow velocity or the depth-integrated velocity at the cell interface are examined. They differ in (1) the character of the transport velocity to bias the discretization of the advective acceleration term in the upwind direction, and (2) the determination of the water depth at the cell face with which the depth-integrated velocity must be linked to the flow velocity. A detailed analysis is provided and aimed at highlighting the necessity of fulfilling the Rankine-Hugoniot jump conditions for preventing the odd-even decoupling problem. The accuracy and robustness of three selected schemes is assessed by means of convergence tests, three idealized 1D test problems with exact solutions and a 1D laboratory experiment of the breaking, runup and rundown of a solitary wave on a sloping beach. Numerical results reveal that schemes satisfying exactly the jump conditions display improved performance over schemes which do not share this property. Also, these results support strong evidence on the link between not fulfilling the jump conditions and the appearance of odd-even oscillations.

Keywords: Shallow water equations, Finite difference schemes, Rankine-Hugoniot relations, Staggered grids, Odd-even decoupling

1. Introduction

The celebrated nonlinear shallow water equations have obtained widespread acceptance for modelling a rich variety of free surface flows in rivers, lakes, floodplains, coastal areas and continental shelves. Such

Email address: m.zijlema@tudelft.nl (Marcel Zijlema)

equations may lead to the formation and propagation of hydraulic discontinuities such as hydraulic jumps, tidal bores, and breaking waves in shallow water [1]. Widely used numerical methods for solving inviscid shallow water equations commonly respect the property of (strict) hyperbolicity of the equations, exploit the features of associated wave characteristics, and rely upon the fully conservative form of the governing equations with the water depth and the depth-integrated velocity as conserved variables. These methods are usually based on a time-explicit, finite volume discretization employing a cell-centred colocated grid arrangement with the aim of computing the inviscid flux at the midpoint of a cell face. Such methods are appropriate for capturing discontinuities in rapidly varied flows. In particular, the Godunov method employing approximate Riemann solvers of Roe [2] and HLL [3] has proven successful. A survey of this vast subject is given in LeVeque [4] and Toro [5].

Although hyperbolic systems admit discontinuous solutions, hyperbolicity is usually the source of problems that arise in developing a numerical scheme for the solution of the shallow water equations. One drawback of this property is related to the numerical imbalance between the pressure flux and the topography term that may appear in the case of discontinuous bed topography. This imbalance leads to artificial flows across sharp bottom gradients in water initially at rest. This numerical artifact may be overcome by constructing a well-balanced scheme that preserves certain kinds of steady state solutions [6–8]. A variety of numerical techniques to achieve the well-balanced property in the Roe and HLL methods is proposed in [9–13]. However, the development of well-balanced schemes can be rather difficult and such schemes are often found to lack robustness in real-life applications. Another difficulty is that strict hyperbolicity is lost if a dry bed is present [14]. Especially the Roe's Riemann solver is not able to cope with problems that involve wet-dry fronts. In addition, dedicated measures are required to avoid non-negativity of the water depth in the case a wet region falling dry. They typically modify the cell variables at the cell face and subsequently the interface flux by means of a hydrostatic reconstruction [7].

The numerical methods mentioned above target to exploit the hyperbolicity property of the governing equations featuring the propagation of wave-like disturbances along the characteristics with a finite speed. Where these characteristics intersect corresponds to a shock or discontinuity, which must satisfy the Rankine-Hugoniot jump relations [1]. They describe the relation between the flow states on both sides of the discontinuity that follow from conservation of mass and momentum. The jump conditions usually express continuity of mass flux and momentum flux across a steady discontinuity (i.e. the shock speed is zero). In this paper we will show that complying with these jump conditions at discretization level warrants the use of numerical schemes which are suitable to solve problems involving (steady) discontinuities, whereas they do not explicitly utilize the hyperbolicity property of the underlying equations. In this context, the flow variables are assumed to be constant in each grid cell or control volume, while treated as discontinuous across the edge of the cell/control volume. Yet it is of crucial importance that the constancy of mass and momentum fluxes across the discontinuity is fulfilled at the discrete level.

Motivated by this observation, any finite difference scheme can, in principle, be employed for the modelling of rapidly varied flows provided that the algebraic Rankine-Hugoniot relations, expressing the continuity of mass flux and momentum flux across the volume edge, are fulfilled. The present study deals with finite difference schemes on staggered Cartesian grids. Such schemes are an attractive alternative to colocated finite volume Godunov-type schemes. The reasons are threefold. First, staggered schemes treat the inviscid flux componentwise and the hyperbolicity feature is ignored. Second, the associated spatial discretization provides simple and accurate approximations and can easily be combined with the implicit ADI-type splitting schemes [15, 16] and semi-implicit $\theta-$methods [17, 18], which are the widely employed time integration techniques due to their large stability region and delicate balance between accuracy and low computational cost. Third, the staggered approach is successfully employed in coastal and ocean modelling of, among others, large-scale barotropic flows, storm surges, stratified flows, flood waves in rivers, inundation by tsunami waves, and morphodynamics in coastal areas in 2D and 3D (see, e.g. [18–22]).

Staggered schemes are not only applicable to subcritical flows, but also suitable for rapidly varied flows. For example, the various staggered grid approaches of Zhou and Stansby [23], Stelling and Duinmeijer [24], Madsen et al. [25], Kramer and Stelling [26], Cui et al. [22], and Doyen and Gunawan [27] to solve shallow water equations yield accurate results for flows at high Froude numbers including hydraulic jumps and dam break problems. In the current work it is explained in detail why these methods are adequate for such flows.

The objective of this paper is twofold. Firstly, it addresses a number of finite difference schemes on staggered grids for the solution of the one-dimensional, depth-integrated, inviscid shallow water equations. These 1D equations served as a basis for identifying a number of numerical issues to be discussed. The current work aims to analyze in-depth the spatial discretization of three staggered schemes, each with a different set of dependent variables, either primitive or conserved, in relation to the Rankine-Hugoniot jump conditions holding across discontinuities. This will shed light on conservation properties of the presented schemes. In this respect, it will be shown that the incompressibility constraint plays a key role in achieving enhanced accuracy and robustness.

The second goal of the paper is to demonstrate how the Rankine-Hugoniot jump conditions can help suppress odd-even spurious modes that would otherwise occur in staggered schemes. In particular, the aim is to show that these conditions are necessary for preventing the odd-even decoupling problem. This turns out to be beneficial for the numerical accuracy and stability of the solution. This forms the basis of our claim that fulfilling the Rankine-Hugoniot relations is to be preferred over exploiting the hyperbolicity property of the governing equations with which a good finite difference scheme should comply.

The rest of this paper is organized as follows. Section 2 briefly reviews the shallow water equations we wish to solve. In this context, it is important to emphasize that incompressibility is a key element in the formulation and discretization of the governing equations. In particular, the analogy with compressible Euler equations of gas dynamics is critically reviewed. The spatial discretization is treated first for a 1D

generic continuity equation in Section 3 and then, in Section 4, for the 1D shallow water equations, by means of a staggered approach, including additional analysis concerning the Rankine-Hugoniot relations. Section 5 outlines the aspects of time integration relevant for the scope of the present study. The performance of three selected schemes is assessed first by means of convergence tests and then by three idealized 1D tests involving flow discontinuities, for which the conservation of mass flux and momentum flux is crucial. In addition, a 1D laboratory experiment of the breaking, runup and rundown of a solitary wave on a sloping beach is used in the assessment. Numerical results are presented to display the comparison between the various schemes. These assessments and outcomes are dealt with in Section 6. Finally, in Section 7, the findings of this study are summarized, followed by a few practical comments upon the implementation of the discussed schemes in two dimensions.

2. Governing equations

We consider the shallow water flow with a free surface under gravity in a Cartesian coordinate system $\boldsymbol{x} = (x, y, z)$. This flow is confined by the surface elevation $z = \zeta(x, y, t)$ (positive upwards with respect to the datum level $z = 0$ with $z-$axis in the direction opposite to that of gravity) and the bed elevation $z = -d(x, y)$ (positive downwards with respect to the datum level), and is uniform in depth. We restrict ourselves to incompressible flows governed by the depth-integrated continuity and momentum equations.

The continuity equation is

$$\frac{\partial h}{\partial t} + \nabla \cdot h\boldsymbol{u} = 0 \tag{1}$$

where $h(x, y, t) = \zeta + d$ is the water depth and $\boldsymbol{u}(x, y, t) = (u, v)$ is the velocity vector with the depth-averaged components u and v along the x and y coordinates, respectively. The mass flux is given by $h\boldsymbol{u}$. Note that in the two-dimensional space (x, y), the divergence operator ∇ reduces to $(\partial/\partial x, \partial/\partial y)$. Eq. (1) is written in divergence form and expresses conservation of volume in the incompressible flow. The Lagrangian form of Eq. (1) reads

$$\frac{Dh}{Dt} = -h\nabla \cdot \boldsymbol{u} \tag{2}$$

with $D/Dt = \partial/\partial t + \boldsymbol{u} \cdot \nabla$ denoting the material derivative. Hence, changes in the water depth that move along with $\boldsymbol{u}$ are associated with divergence of the flow velocity $\boldsymbol{u}$. This is the case with, for instance, spatial variations of the seabed.

The momentum equation is

$$\frac{\partial \boldsymbol{q}}{\partial t} + \nabla \cdot \left(\boldsymbol{u} \otimes \boldsymbol{q} + \frac{1}{2} g h^2 \boldsymbol{I} \right) = gh\nabla d \tag{3}$$

where $\boldsymbol{q} = h\boldsymbol{u}$ is the depth-integrated velocity (momentum per unit area normalised by the density), g is the gravitational acceleration, and $\boldsymbol{I}$ is the identity matrix. The momentum flux is given by $\boldsymbol{u} \otimes \boldsymbol{q} + \frac{1}{2} g h^2 \boldsymbol{I}$ and the pressure is assumed to be hydrostatic. Eq. (3) merely maintains its conservative character in the absence

of the source term, i.e. the bed is supposed to be uniform. It is worth commenting that the depth-integrated velocity $\boldsymbol{q}$ in Eq. (3) and the mass flux $h\boldsymbol{u}$ in Eq. (1) are different in their role: the former is a storage quantity, whereas the latter one is a transport quantity.

The continuity equation (1) and the momentum equation (3) are the well-known inviscid shallow water equations in strong conservation form for the solution of h and $\boldsymbol{q}$ being the conserved variables. Initially smooth h and $\boldsymbol{q}$ may become discontinuous within finite time. These shocks propagate at speeds determined by the Rankine-Hugoniot relations arising from the conservation of mass and momentum [4]. Various Godunov-type methods have been devised for the numerical solution of this system of nonlinear hyperbolic equations that is mathematically equivalent to the compressible Euler equations of gas dynamics [4, 5]. Applications of approximate Riemann solvers to shallow water equations, such as Roe [2] and HLL [3], are found in, e.g. [9, 12–14, 28]. Furthermore, alternative methods have been proposed that avoid the necessity to solve a Riemann problem. Examples are the TVD-MacCormack scheme [29], the central-upwind method [6], the artificial viscosity approach [30], and energy stable schemes using numerical diffusion operators based on entropy variables [8]. Typically, the abovementioned methods employ colocated variable arrangement: both h and $\boldsymbol{q}$ are stored at the same set of grid nodes.

For reasons that become clear later on, the preferred form of the shallow water equations for incompressible flow is

$$\frac{\partial \zeta}{\partial t} + \nabla \cdot \boldsymbol{q} = 0 \tag{4}$$

$$\frac{\partial h\boldsymbol{u}}{\partial t} + \nabla \cdot (\boldsymbol{q} \otimes \boldsymbol{u}) + gh\nabla\zeta = 0 \tag{5}$$

with the primitive variables ζ and $\boldsymbol{u}$. These equations are written in weak conservation form without a splitting of the surface gradient into a pressure flux and a source term that includes the effect of the bed slope (cf. Eq. (3)). We thus refrain from using the hyperbolicity property. Nonetheless, for large-scale applications in coastal and ocean engineering, the governing equations are usually written in the following non-conservation form

$$\frac{\partial \zeta}{\partial t} + \nabla \cdot h\boldsymbol{u} = 0$$

$$\frac{\partial \boldsymbol{u}}{\partial t} + (\boldsymbol{u} \cdot \nabla)\ \boldsymbol{u} = -g\nabla\zeta$$

whereas other relevant forces should be included, such as the frictional forces (wind shear and bottom roughness) and the Coriolis force due to the Earth's rotation. Different numerical methods have been proposed for the solution of these shallow water equations; see, e.g. [15–21, 31]. These methods all have in common that they employ staggered grids: the primitive variables are stored at alternate locations; the water level is stored at a cell centre, and the velocity is stored at a cell face. Using this variable storage arrangement is an effective way to avoid odd-even decoupling between the surface elevation and flow velocity.

Although the mathematical structure of Eqs. (1) and (3) is equivalent to that of the Euler equations of gas dynamics, being a system of hyperbolic conservation laws for which Godunov-type methods are applicable, a crucial difference is the physical behaviour of the flow field. The *compressible* Euler equations are classified as hyperbolic and examples of flows governed by these equations are unsteady sub- and supersonic flows and steady supersonic flows [32]. On the other hand, the inviscid shallow water equations have been derived from depth integration of the *incompressible* Euler equations and the associated flow behaviour is of elliptic nature due to the incompressibility constraint [32]. Much in the same way, Eqs. (4) and (5) are hyperbolic for unsteady flows and but elliptic for steady flows. Examples of the latter are rapidly varied steady flows (e.g. flow over a weir crest and flow through an orifice)[1]. Yet, for steady state solutions, the continuity equation (4) degenerates to a constraint $\nabla \cdot \boldsymbol{q} = 0$, i.e. the depth-integrated velocity is a solenoidal field. This constraint can be dealt with effectively by the use of staggered grids. This also applies for unsteady flows. Examples of (un)steady flows with sudden changes in the bathymetry will be presented in Section 6.3.

Further to this, Eq. (3) is a transport equation for the variable $\boldsymbol{q}$, which is the advected quantity, whereas $\boldsymbol{u}$ acts as transport velocity. This is also reflected in the second term of Eq. (3),

$$\nabla \cdot (\boldsymbol{u} \otimes \boldsymbol{q}) = (\boldsymbol{u} \cdot \nabla)\ \boldsymbol{q} + h\,(\nabla \cdot \boldsymbol{u})\ \boldsymbol{u}$$

where the first term on the right hand side is related to the background flow. The second term is closely linked to the change in the water depth along flow paths (viz. Eq. (2)), illustrating how the change in the depth-integrated velocity $\boldsymbol{q}$ and the change in the water depth h are intertwined. Yet Eqs. (1) and (3) are a set of hyperbolic equations, and thus attractive as they lend themselves to diagonalization yielding distinct variables along their characteristics.

Eqs. (4) and (5), on the other hand, naturally describe the propagation of gravity waves as the essential terms are the surface gradient, i.e. the third term of Eq. (5), and the divergence of the mass flux, i.e. the second term of Eq. (4). Observe that the divergence term of Eq. (5) includes two parts, $(\boldsymbol{q} \cdot \nabla)\ \boldsymbol{u}$ and $(\nabla \cdot \boldsymbol{q})\ \boldsymbol{u}$, of which the second part is commonly related to the wave propagation (viz. Eq. (4)). Hence, the combination of terms $(\nabla \cdot \boldsymbol{q})\ \boldsymbol{u}$ and $gh\nabla\zeta$ in the momentum equation characterizes the wave-like propagation on top of the background flow. The first part of the divergence term represents advection in the background flow. This implies that the depth-averaged velocity $\boldsymbol{u} = \boldsymbol{q}/h$ is transported by the mass flux $\boldsymbol{q}$, like volume (or mass). This transported velocity $\boldsymbol{u}$ is thus the resolved variable of the depth-integrated momentum equation (5). This feature turns out to be beneficial for accuracy and stability as will be demonstrated in the current study.

In this paper it is argued that the model based on Eqs. (4) and (5) can preserve shocks and discontinuities, if the underlying numerical scheme complies with some form of discrete conservation that enables to compute

[1]The associated pressure distribution may not be hydrostatic in the region of curved flows.

shocks with the correct speed. Yet, rather than conservation itself, it would be crucial for physical accuracy to employ a discrete form of the Rankine-Hugoniot jump conditions which relate the fluid states on both sides of a discontinuity. Thereby, a finite difference scheme that relies upon this type of conservation form is able to produce the correct weak solution to the aforementioned equations. This is the central theme of this paper.

3. Finite difference schemes for a 1D generic continuity equation

Before we outline various numerical methods for the solution of the shallow water equations, we first discuss the spatial discretization of a generic continuity equation to demonstrate the basic ideas of the different numerical approximations to follow with some useful observations. The numerical approach to the shallow water equations will be developed later in Section 4.

A generic continuity equation is a special case of a conservation law (see [4]), and is given in one-dimensional form as follows

$$\frac{\partial c}{\partial t} + \frac{\partial uc}{\partial x} = 0$$

where $c(x,t)$ is a conserved variable and $u(x,t)$ is the flow velocity. This equation typically expresses conservation of quantity c (e.g. mass, volume, internal energy), implying that the rate of change of its amount within a closed surface is merely due to the flux $f(c) = uc$ across the surface. If the net flux is zero, like in an isolated system, then c does not change over time.

We define a computational grid in the $x-$space discretized in M grid cells. A part of this computational grid is depicted in Figure 1. Within this grid we have cell centres located at x_m, with $m = 1, ..., M$, and

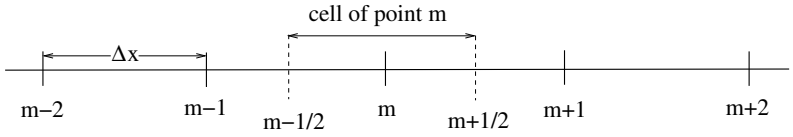

Figure 1: A part of a 1D computational grid.

cell interfaces at $x_{m+1/2}$, with $m = 0, ..., M$. We assume an equidistant grid with a constant grid size Δx. The grid cells can be regarded as control volumes containing densities $c_m(t) \approx c(x_m, t)$. Their discrete values represent piecewise constant averages of the densities over the cells. Consequently, the densities are discontinuous across cell interfaces.

The desired semi-discretized equation must reflect the conservation property in the sense that c_m can only be reduced by moving some of it to neighbouring cells. Or its amount can be enlarged by moving something from neighbouring cells into cell m. Hence, the temporal variation of c_m can be seen as in- and outflow through the cell interfaces. This is expressed in terms of a face flux $f_{m+1/2} = f(c_{m+1/2}) \approx f(c(x_{m+1/2}, t))$

and naturally, we get the next balance principle

$$\Delta x \frac{dc_m}{dt} = f_{m-1/2} - f_{m+1/2} \tag{6}$$

which yields the following semi-discretized formulation

$$\frac{dc_m}{dt} + \frac{f_{m+1/2} - f_{m-1/2}}{\Delta x} = 0$$

Note that the balance equation (6) can also be derived from the application of the finite volume method. This method is designed to obtain a correct weak solution through, among others, the conservation requirement [4, 33]. Although global conservation can easily be obtained with any finite volume scheme, due to the natural cancellation of fluxes in the interior of the domain, the question remains how to determine the numerical flux at the cell interface, as the density c is not known at the cell interfaces. This is the central issue being addressed in the finite volume method: to express the cell-face value in terms of cell-centre values. Interpolation thus determines the variation of the conserved quantity c between cell centroids. Below, we will see that the choice of interpolation will affect both accuracy and stability of the numerical method. This is particularly the case for hyperbolic PDEs with discontinuous solutions. On the contrary, global conservation proves to be more relevant to a convection-diffusion type equation for which the option of flux interpolation is less critical anyway. This is especially the case when there are no sources and sinks. In such a case, telescopic cancelling of internal fluxes would be rather beneficial.

By employing a staggered variable arrangement the discrete scalars c are resided in cell centres as defined before, but the discrete velocities u are positioned at the cell faces. Their values are designated by $u_{m+1/2}$, with $m = 0, ..., M$. To demonstrate proper treatment of a discontinuity at the discrete level, we consider a stationary flow. This case is motivated by the requirement of flux conservation, as becomes clear later on. We have the following spatial discretization

$$\frac{f_{m+1/2} - f_{m-1/2}}{\Delta x} = \frac{u_{m+1/2}c_{m+1/2} - u_{m-1/2}c_{m-1/2}}{\Delta x} = 0 \tag{7}$$

The density c at the faces of the control volume needs to be interpolated in terms of cell-centre values. Linear interpolation or arithmetic averaging is the commonly used one and is given by

$$c_{m+1/2} \approx \frac{1}{2}\left(c_m + c_{m+1}\right)$$

Substitution yields a second order scheme for a uniform grid,

$$0 = \frac{f_{m+1/2} - f_{m-1/2}}{\Delta x} \approx \frac{u_{m+1/2}\left(c_m + c_{m+1}\right) - u_{m-1/2}\left(c_{m-1} + c_m\right)}{2\Delta x} \tag{8}$$

This scheme can give rise to a spurious checkerboard mode for density c. Indeed, if the flow velocity is divergence free or uniform, i.e. $u_{m+1/2} = u_{m-1/2}$, we obtain

$$c_{m+1} = c_{m-1}$$

which involves alternate c values only, allowing unwanted oscillations with a wave length of $2\Delta x$, $c_m = (-1)^m \tilde{c}$ with $d\tilde{c}/dx = 0$. This odd-even decoupling is not detected by the scheme and, as a consequence, the checkerboard mode can be unbounded.

To prevent spurious oscillations, a first order upwind scheme is chosen, as follows

$$c_{m+1/2} \approx \begin{cases} c_m \,, & \text{if } u_{m+1/2} > 0 \\ \\ c_{m+1} \,, & \text{if } u_{m+1/2} < 0 \end{cases} \tag{9}$$

Let us consider a positive flow. One obtains

$$0 = \frac{f_{m+1/2} - f_{m-1/2}}{\Delta x} \approx \frac{u_{m+1/2} c_m - u_{m-1/2} c_{m-1}}{\Delta x} \tag{10}$$

which clearly cured the odd-even decoupling problem.

We reexamine the schemes (8) and (10) but from a different point of view, namely conservation of a flux. Certain physical quantities may undergo rapid changes leading to the formation of a shock in a finite time. For instance, discontinuous water depths and flow velocities may occur in rapidly varied flows like flows over steep bottom slopes, hydraulic jumps, tidal bores, and broken waves. On the other hand, continuity is required regarding to the flow or transport across an abrupt change. This can readily be deduced from the Rankine-Hugoniot relation or jump condition [1].

Let us consider a stationary jump at $x_1 < x_s < x_2$, where the subscripts 1 and 2 denote just upstream and just downstream of the jump, respectively. Although the quantities c and u may exhibit a discontinuity at x_s, flux uc must be continuous across the jump, since $d\,uc/dx = 0$. Hence, the following flux conservation must hold

$$u_1\, c_1 = u_2\, c_2 \tag{11}$$

Commonly, condition (11) enforces conservation of flux across the shock. However, this condition can also be interpreted as a prerequisite for an accurate and stable approximation of the flux at the cell interface. By nature, discrete unknowns are piecewise constant functions on a computational grid, and consequently, are discontinuous across cell faces. Generally, their smoothness properties are influenced by the grid resolution. In turn, this may affect the numerical accuracy. Variations in u and c, particularly across shocks, tend to be far stronger than changes in flux uc. Furthermore, since grid cells on either side of a discontinuity contain no information about each other, any approximation of unknown c using arithmetic averaging, linear interpolations or central discretizations can give rise to spurious oscillations. Yet it is desirable that Eq. (11) holds exactly at the discrete level; given the upstream state of the flow, the downstream state is completely determined by the Rankine-Hugoniot relation in question. Hence, numerical errors associated with inadequate resolution of gradients are reduced significantly, whereas stability might enhanced as the odd-even decoupling of any dependent variable may be prevented. However, as we will see in due course,

when a numerical scheme does not comply with the jump condition (11), the odd-even decoupling problem crops up, if allowed by the scheme.

Let us go back to our schemes. From Eq. (10) we have

$$u_{m+1/2}\, c_m = u_{m-1/2}\, c_{m-1}$$

implying that flux uc is continuous when evaluated from either side of the cell. This scheme strictly conserves flux cell by cell and remains accurate irrespective of the grid size. This is called cellwise (or pointwise) conservation and the associated jump condition is given by

$$[uc]_m = u_{m+1/2}\, c_m - u_{m-1/2}\, c_{m-1} = 0 \tag{12}$$

with the operator $[\cdot]_m$ denoting the jump of a flux across cell m.

By contrast, from Eq. (8), we derive the following

$$[uc]_m = u_{m+1/2}\, c_m - u_{m-1/2}\, c_{m-1} = u_{m-1/2}\, c_m - u_{m+1/2}\, c_{m+1} \tag{13}$$

Obviously, continuity of flux uc across the cell can not be obtained by the achieved scheme as the right hand side gives rise to internal sources of density c. This is the case, for instance, if the flow velocity u is divergence free and density c exhibits an odd-even oscillation. To appreciate the nature of the underlying problem, it should be pointed out that the magnitude of the error due to disbalance (13) can be relevant, especially when a coarse grid is employed. Provided this scheme is converging, one can obviously achieve a high accuracy by refining the mesh, but this approach is untenable in large-scale simulations.

4. Finite difference schemes for the 1D shallow water equations

This section deals with the various spatial discretizations of the inviscid, incompressible shallow water equations. In order to make the matter clear and unambiguous, but with no loss of generality, we will present a detailed study of the different methods applied to the one-dimensional continuity and momentum equations. We will discuss two versions of these equations in the remainder of this paper. The first system of equations to be investigated is given by

$$\frac{\partial \zeta}{\partial t} + \frac{\partial q}{\partial x} = 0 \tag{14}$$

$$\frac{\partial hu}{\partial t} + \frac{\partial qu}{\partial x} + gh\frac{\partial \zeta}{\partial x} = 0 \tag{15}$$

with the primitive variables $\zeta(x,t)$ and $u(x,t)$. Furthermore, $h(x,t) = \zeta(x,t) + d(x)$ and $d(x)$ represents the bed topography. These one-dimensional equations follow from Eqs. (4) and (5), respectively. The second one is a set of hyperbolic equations based on Eqs. (1) and (3), and is given in 1D form

$$\frac{\partial h}{\partial t} + \frac{\partial q}{\partial x} = 0 \tag{16}$$

$$\frac{\partial q}{\partial t} + \frac{\partial \left(uq + \frac{1}{2} g h^2 \right)}{\partial x} = gh \frac{\partial d}{\partial x} \tag{17}$$

with the flux variables $h(x,t)$ and $q(x,t)$.

Each of the above sets of 1D equations serves as a proxy for a detailed analysis of the different numerical approaches to be discussed below. We will first consider the spatial discretization of continuity equation (14) and momentum equation (15). Thereafter, the discretization of the hyperbolic equations (16) and (17) will be outlined. Time integration will be presented in Section 5.

With the staggered grid arrangement, the primitive variables are carried at alternate grid points. Both the water level ζ_m and water depth h_m are located at the cell centre of the associated grid cell, x_m, whereas this grid cell is bounded by the cell interfaces at $x_{m-1/2}$ and $x_{m+1/2}$, where the velocities $u_{m\pm1/2}$ are located; see also Figure 1. Note that the bed level d_m is resided at the cell centre.

A two-point stencil can be obtained for both the continuity equation and all terms of the momentum equation, except the advection term, approximated with second order accuracy on staggered uniform meshes. This provides the ability to construct numerical schemes that are consistent with the Rankine-Hugoniot relations for conservation of mass flux and momentum flux.

Let us consider the continuity equation (14). Central discretization in space yields

$$\frac{d\zeta_m}{dt} + \frac{q_{m+1/2} - q_{m-1/2}}{\Delta x} = 0 \tag{18}$$

For a stationary flow, we have

$$q_{m+1/2} - q_{m-1/2} = 0 \Rightarrow$$

$$[q]_m = 0 \tag{19}$$

Eq. (19) represents the Rankine-Hugoniot relation with respect to the cellwise conservation of mass flux applied at the staggered grid.

Since $u_{m+1/2}$ is the primitive variable, we compute the mass flux, as follows

$$q_{m+1/2} = h_{m+1/2} u_{m+1/2} \tag{20}$$

The water depth at the cell face $h_{m+1/2}$ must be defined further. The following first order approximation allows conditional preservation of non-negativity of the water depth (see Section 5)

$$h_{m+1/2} \approx \hat{h}_{m+1/2} = \begin{cases} h_m \,, & \text{if } u_{m+1/2} > 0 \\ \\ h_{m+1} \,, & \text{if } u_{m+1/2} < 0 \end{cases} \tag{21}$$

with the hat denoting an upwind value. Alternatively, the surface elevation ζ can be taken upwind instead of the water depth h, while the bed level d is determined by means of a min operator (see, for instance, [34]).

This may lead to a more accurate result, particularly at coarse grids. In this study, however, we restrict ourselves to the use of Eq. (21). This completes the spatial discretization of the continuity equation.

Next, we consider the second term of the momentum equation (15). We have assumed an equidistant grid in the $x-$space, and we do not consider the domain boundaries. Due to these assumptions, and the fact that the considered term is written in a conservative form, both finite difference and finite volume methods yield the same discretization, which is given by

$$\frac{\partial qu}{\partial x}|_{m+1/2} \approx \frac{(qu)_{m+1} - (qu)_m}{\Delta x} \tag{22}$$

with $m + 1/2$ the index indicating the cell-centre point in a control volume of $u_{m+1/2}$. The faces of this control volume are indicated with the indices m and $m + 1$. In this context, the velocity of momentum $u_{m+1/2}$ is a cell-volume quantity, whereas the mass flux $q_{m+1/2}$ in Eq. (20) is a cell-face quantity. Both q and u at the faces of the control volume need to be interpolated. Since the mass flux q is continuous, the following interpolation

$$q_m \approx \overline{q}_m = \frac{1}{2}\left(q_{m-1/2} + q_{m+1/2}\right) \tag{23}$$

is a proper one. Here, the overbar denotes the aritmethic average of a quantity across the cell or cell interface. This averaging is second order accurate on a uniform grid. For the transported velocity u_m (it may not be smooth!) we apply a first order upwind scheme, as follows

$$u_m \approx \hat{u}_m = \begin{cases} u_{m-1/2}\,, & \text{if } \overline{q}_m > 0 \\ \\ u_{m+1/2}\,, & \text{if } \overline{q}_m < 0 \end{cases} \tag{24}$$

Second order accuracy can be obtained by means of a higher order upwind scheme, with or without a flux limiter. This scheme is treated as a deferred correction to the first order upwind scheme, while this correction is added to the right hand side of the momentum equation [35]. In this way, second order accuracy is achieved, and the size of the stencil associated with the first order upwind scheme is unaltered and remains low.

The approximation of the third term of Eq. (15) is obtained by means of second order central differences, as follows

$$h\,\frac{\partial \zeta}{\partial x}|_{m+1/2} \approx \overline{h}_{m+1/2}\frac{\zeta_{m+1} - \zeta_m}{\Delta x}$$

with

$$\overline{h}_{m+1/2} = \frac{1}{2}\,(h_m + h_{m+1}) \tag{25}$$

To demonstrate cellwise conservation of the momentum flux, we thus restrict ourselves to a stationary, positive flow. In this case q is constant, and so we have $\overline{q}_m = q_{m-1/2} = q_{m+1/2}$, and with $\overline{q}_m > 0$ and $\overline{q}_{m+1} > 0$, one obtains from Eq. (22)

$$\frac{\partial qu}{\partial x}|_{m+1/2} \approx \frac{\overline{q}_{m+1}\hat{u}_{m+1} - \overline{q}_m\hat{u}_m}{\Delta x} = \frac{q_{m+1/2}u_{m+1/2} - q_{m-1/2}u_{m-1/2}}{\Delta x} \tag{26}$$

We prove the cellwise conservation of momentum flux as follows

$$q_{m+1/2}u_{m+1/2} - q_{m-1/2}u_{m-1/2} + g\overline{h}_{m+1/2}\left(\zeta_{m+1} - \zeta_m\right) = 0 \Rightarrow$$

$$q_{m+1/2}u_{m+1/2} - q_{m-1/2}u_{m-1/2} + g\overline{h}_{m+1/2}\left(h_{m+1} - h_m\right) = g\overline{h}_{m+1/2}\left(d_{m+1} - d_m\right) \Rightarrow$$

$$q_{m+1/2}u_{m+1/2} - q_{m-1/2}u_{m-1/2} + \frac{1}{2}g\left(h_{m+1}^2 - h_m^2\right) = g\overline{h}_{m+1/2}\left(d_{m+1} - d_m\right) \Rightarrow$$

$$\left[qu + \frac{1}{2}gh^2\right]_{m+1/2} = g\overline{h}_{m+1/2}\left[d\right]_{m+1/2} \tag{27}$$

Eq. (27) represents the Rankine-Hugoniot relation of momentum flux conservation applied at the staggered grid. Note that this relation holds on the interface $x_{m+1/2}$, while the jump in qu is taken upstream of cell edge $x_{m+1/2}$ by virtue of flux continuity (cf. Eq. (12)). It must be emphasized that this property remains valid when second order accuracy by means of a deferred correction scheme is included. It should also be noted that the water depth at the cell face, Eq. (25) as occurred in the surface gradient, is taken as the arithmetic average. This is required to obtain a well-balanced scheme representing the hydrostatic balance between the pressure flux and the topography term [7, 10]

$$\frac{1}{2}g\left[h^2\right]_{m+1/2} = g\overline{h}_{m+1/2}\left[d\right]_{m+1/2} \tag{28}$$

that enables to preserve the quiescent water over varying bathymetry, i.e. ζ = constant, and $u = 0$.

Continuity of the mass flux and momentum flux across a discontinuity, as given by Eqs. (19) and (27), respectively, requires a loss in the (kinetic) energy (implying an increase of entropy)[2] [1]. This loss is due to the viscous dissipation and is provided by the upwind scheme (24). This numerical viscosity is also required to damp out oscillations arising in the regions of steep gradients and numerical dispersion errors. Although numerical viscosity is an implicit and uncontrollable feature of the applied upwind scheme, the corresponding value of viscosity is solely determined by the cellwise conservation of mass and momentum fluxes across the discontinuity. This implies a correct magnitude needed for a viscosity to handle the discontinuities in the primitive variables. This will be demonstrated in Section 6.3.1.

The above approximations are outlined and proposed earlier in [24] and [27]. They are also implemented in NEOWAVE [36] and SWASH [34]. In addition, similar discretization equations were presented by Zhou [37], although he suggested to apply Eq. (25), instead of Eq. (21), to approximate the mass flux following Eq. (20). It must be stressed that, contrary to the approaches of Doyen and Gunawan [27] and Zhou [37], the spatial discretizations presented so far have been obtained from equations that are not written in strong conservation form, viz. Eqs. (14)−(15). In fact, they can even be derived from shallow water equations in non-conservative form (see, e.g. [24]).

[2] As such, a flow across the discontinuity experiences a deceleration. That is to say, the combined approximations (19) and (27) can not be applied in regions of contraction with flow acceleration. For instance, Stelling and Duinmeijer [24] demonstrated an erroneous increase in energy head for the subcritical flow over sudden contractions due to strict conservation of momentum.

We now construct a staggered scheme for the solution of continuity and momentum equations written in strong conservation form, viz. Eqs. (16) and (17). The momentum variable q is considered as the unknown of the momentum equation (17), which is the local momentum per unit length, whereas $u = q/h$ is the flow rate per unit width. Obviously, q is treated as the transported storage quantity, whereas u acts as transport velocity. This point of view has been adopted by, among others, Stansby [18] and Zijlema and Stelling [38]. The continuity equation (16) is discretized as

$$\frac{dh_m}{dt} + \frac{q_{m+1/2} - q_{m-1/2}}{\Delta x} = 0 \tag{29}$$

which satisfies the jump condition (19) in steady-state case.

For spatial discretization of the advection term of Eq. (17), first order upwinding with respect to q is employed, while taking the arithmetic mean of u, as follows

$$\frac{\partial uq}{\partial x}|_{m+1/2} \approx \frac{(uq)_{m+1} - (uq)_m}{\Delta x} \tag{30}$$

with

$$u_m \approx \overline{u}_m = \frac{1}{2}\left(u_{m-1/2} + u_{m+1/2}\right) \tag{31}$$

and

$$q_m \approx \hat{q}_m = \begin{cases} q_{m-1/2}\,, & \text{if } \overline{u}_m > 0 \\ \\ q_{m+1/2}\,, & \text{if } \overline{u}_m < 0 \end{cases} \tag{32}$$

The other terms of Eq. (17) are discretized centrally, as follows

$$\frac{\partial h^2}{\partial x}|_{m+1/2} \approx \frac{h^2_{m+1} - h^2_m}{\Delta x}$$

and

$$h\frac{\partial d}{\partial x}|_{m+1/2} \approx \overline{h}_{m+1/2}\frac{d_{m+1} - d_m}{\Delta x}$$

Velocity $u_{m+1/2}$ remains to be defined, since $q_{m+1/2}$ is the resolved variable. Stansby [18] suggested the following 'central' approach

$$u_{m+1/2} = \frac{q_{m+1/2}}{\overline{h}_{m+1/2}} \tag{33}$$

However, as an alternative, this quantity may also be obtained from Eqs. (20) and (21), as follows

$$u_{m+1/2} = \frac{q_{m+1/2}}{\hat{h}_{m+1/2}} \tag{34}$$

which is referred to as the 'upwind' approach. Note that $u_{m+1/2}$ may not be smooth for flow with space-varying depth.

We now demonstrate that the jump condition can not be guaranteed. Let us consider a steady-state, positive flow. We have $q_{m+3/2} = q_{m+1/2} = q_{m-1/2}$, and

$$\begin{aligned}\frac{\partial uq}{\partial x}|_{m+1/2} &\approx \frac{\overline{u}_{m+1}\hat{q}_{m+1} - \overline{u}_m\hat{q}_m}{\Delta x} = \\ &= \frac{\left(u_{m+1/2} + u_{m+3/2}\right) q_{m+1/2} - \left(u_{m-1/2} + u_{m+1/2}\right) q_{m-1/2}}{2\Delta x} \\ &= \frac{\frac{1}{2}\left(u_{m+3/2} + u_{m-1/2}\right) q_{m+1/2} - u_{m-1/2}q_{m-1/2}}{\Delta x} \end{aligned} \tag{35}$$

Substitution in the discretized momentum equation yields

$$\left(\frac{u_{m+3/2} + u_{m-1/2}}{2}\right) q_{m+1/2} - u_{m-1/2}q_{m-1/2} + \frac{1}{2}g\left(h_{m+1}^2 - h_m^2\right) = g\overline{h}_{m+1/2}\left(d_{m+1} - d_m\right) \tag{36}$$

Thus, the jump condition (27) can not be recovered exactly at the staggered grid due to an arithmetic averaging of flow velocity at $x_{m+1/2}$. In fact, $u_{m+1/2}$ is not involved in Eq. (36), indicating that this scheme allows odd-even decoupling. This will lead to inaccurate momentum flux, as will be demonstrated in Section 6.

The cause is the reverse roles of the transported quantity and the transport velocity. In this approach, they are q and u, respectively, which should be the other way around, i.e. u and q, because of the constraint $\partial q/\partial x = 0$. Indeed, q is constant across a grid cell that is assured by the continuity equation (19). Next, if $\partial(qu)/\partial x = 0$, then u must be constant. Using the discretization according to Eq. (26) yields

$$u_{m+1/2} = u_{m-1/2}$$

implying that u is constant over the same cell. However, with approximation (35), one obtains

$$u_{m+3/2} = u_{m-1/2}$$

displaying the odd-even decoupling, which induces a checkerboard pattern.

5. Time integration

The staggered schemes, as outlined in Section 4, are integrated in time by means of an explicit leapfrog scheme using staggering in time [31]. The flow velocity $u_{m+1/2}$ and the depth-integrated velocity $q_{m+1/2}$ are evaluated at each half time step $(n+1/2)\Delta t$, whereas the surface elevation ζ_m and the water depth h_m at each whole time step $n\Delta t$, with Δt the time step and $n = 0, ..., N$ indicating the time level $t^n = n\Delta t$ with, in total, $N+1$ time steps.

We consider three variants of the staggered schemes to be integrated in time.

Variant I

The first variant has been discussed earlier in Doyen and Gunawan [27]. They first solve the continuity equation to obtain h_m^{n+1}, followed by the momentum equation to obtain $u_{m+1/2}^{n+3/2}$. Hence, the continuity equation (29) is discretized in time, as follows

$$\frac{h_m^{n+1} - h_m^n}{\Delta t} + \frac{q_{m+1/2}^{n+1/2} - q_{m-1/2}^{n+1/2}}{\Delta x} = 0 \tag{37}$$

This equation represents the volume balance

$$\Delta x \left[h_m^{n+1} - h_m^n\right] + \Delta t \left[q_{m+1/2}^{n+1/2} - q_{m-1/2}^{n+1/2}\right] = 0$$

demonstrating that the volume (per unit width) is conserved over time for an isolated physical domain. Furthermore, with $q_{m+1/2}^{n+1/2} = \hat{h}_{m+1/2}^n u_{m+1/2}^{n+1/2}$, one can verify by insertion of Eq. (21) into Eq. (37) that the water depth h_m^{n+1} remains non-negative [24], if

$$\frac{\left[\max\left(u_{m+1/2}^{n+1/2}, 0\right) - \min\left(u_{m-1/2}^{n+1/2}, 0\right)\right] \Delta t}{\Delta x} \leq 1 \tag{38}$$

Condition (38) is a sufficient but not necessary condition. By virtue of Eq. (21), the water depth at the cell interface, $\hat{h}_{m+1/2}^{n+1}$, is non-negative under the same condition. Thus, flooding never happens faster than one grid cell per time step. On the other hand, when a wet cell becomes dry, the water depth can be arbitrary small, making the solution of the momentum equation meaningless. Instead, the momentum equation (39) is not solved and the velocity $u_{m+1/2}^{n+3/2}$ is set to zero if the water depth $\hat{h}_{m+1/2}^{n+1}$ is below a threshold value. Throughout this work, this value equals 10^{-8} m, which does not adversely affect the mass balance. Apart from this minor measure, no further modifications with respect to wetting and drying are required.

The time-integrated version of the momentum equation, as proposed by Doyen and Gunawan [27], is given by

$$\begin{aligned} \frac{\overline{h}_{m+1/2}^{n+1} u_{m+1/2}^{n+3/2} - \overline{h}_{m+1/2}^{n} u_{m+1/2}^{n+1/2}}{\Delta t} &+ \frac{\overline{q}_{m+1}^{n+1/2} \hat{u}_{m+1}^{n+1/2} - \overline{q}_{m}^{n+1/2} \hat{u}_{m}^{n+1/2}}{\Delta x} + \frac{1}{2} g \frac{(h_{m+1}^{n+1})^2 - (h_m^{n+1})^2}{\Delta x} \\ &= g\, \overline{h}_{m+1/2}^{n+1} \frac{d_{m+1} - d_m}{\Delta x} \end{aligned} \tag{39}$$

or, alternatively,

$$\frac{\overline{h}_{m+1/2}^{n+1} u_{m+1/2}^{n+3/2} - \overline{h}_{m+1/2}^{n} u_{m+1/2}^{n+1/2}}{\Delta t} + \frac{\overline{q}_{m+1}^{n+1/2} \hat{u}_{m+1}^{n+1/2} - \overline{q}_{m}^{n+1/2} \hat{u}_{m}^{n+1/2}}{\Delta x} + g\, \overline{h}_{m+1/2}^{n+1} \frac{\zeta_{m+1}^{n+1} - \zeta_m^{n+1}}{\Delta x} = 0 \tag{40}$$

with $\zeta_m^{n+1} = h_m^{n+1} - d_m$. Note that the third term is evaluated using the updated h_m^{n+1} to obtain a stable solution [27], and that no systems of equations are involved. The second term of Eq. (39) is evaluated by means of Eqs. (23) and (24). Notice the role of mass flux q in Eq. (39) being the transport velocity. Assuming a uniform bed, the momentum balance can be derived from Eq. (39), yielding

$$\Delta x \left[q_{m+1/2}^{n+3/2} - q_{m+1/2}^{n+1/2}\right] + \Delta t \left[\overline{q}_{m+1}^{n+1/2} \hat{u}_{m+1}^{n+1/2} - \overline{q}_{m}^{n+1/2} \hat{u}_{m}^{n+1/2} + \frac{1}{2} g \left((h_{m+1}^{n+1})^2 - (h_m^{n+1})^2\right)\right] = 0$$

provided that $q_{m+1/2}^{n+1/2} = \overline{h}_{m+1/2}^{n} u_{m+1/2}^{n+1/2}$ is the conserved momentum per unit length.

The time step for this explicit scheme is limited by the following CFL criterion

$$\frac{\left[\mid u_{m+1/2}^{n+1/2} \mid + \sqrt{g\hat{h}_{m+1/2}^{n}}\right] \Delta t}{\Delta x} \leq 1$$

Note that this CFL criterion determines the maximum time step which satisfies automatically condition (38).

Variant II

The second variant resembles the first one in the solution procedure, except that the momentum per unit length q is updated instead of flow velocity u, by solving the following equation

$$\frac{q_{m+1/2}^{n+3/2} - q_{m+1/2}^{n+1/2}}{\Delta t} + \frac{\overline{u}_{m+1}^{n+1/2} \hat{q}_{m+1}^{n+1/2} - \overline{u}_{m}^{n+1/2} \hat{q}_{m}^{n+1/2}}{\Delta x} + \frac{1}{2} g \frac{(h_{m+1}^{n+1})^2 - (h_{m}^{n+1})^2}{\Delta x} = g\, \overline{h}_{m+1/2}^{n+1} \frac{d_{m+1} - d_m}{\Delta x} \quad (41)$$

which conserves $q_{m+1/2}^{n+3/2}$ in the case of a uniform bed topography. The second term of Eq. (41) is evaluated using Eqs. (31) and (32). Since q is the resolved variable, the requirement of strict non-negative water depths can not be properly enforced by Eq. (37). In addition, q is the transported quantity, whereas u is the transport velocity which needs to be reconstructed, either based on Eq. (33) or Eq. (34). Like the first variant, a no flow condition at the cell interface between a dry and wet cell is imposed, so that the mass balance is maintained.

A similar approach in which the local momentum q is updated can be found in Madsen et al. [25].

Variant III

SWASH is a wave-flow model intended to simulate both long and short waves and rapidly varied flows [34]. This model solves the shallow water equations including the non-hydrostatic pressure that takes into account the frequency dispersion of the short waves and vertical accelerations. For this reason, and contrary to the first variant, in this variant the momentum equation is solved first and then the continuity equation. We will deal with the following explicit momentum equation (cf. Eq. (40))

$$\frac{\overline{h}_{m+1/2}^{n} u_{m+1/2}^{n+1/2} - \overline{h}_{m+1/2}^{n-1} u_{m+1/2}^{n-1/2}}{\Delta t} + \frac{\overline{q}_{m+1}^{n-1/2} \hat{u}_{m+1}^{n-1/2} - \overline{q}_{m}^{n-1/2} \hat{u}_{m}^{n-1/2}}{\Delta x} + g\, \overline{h}_{m+1/2}^{n} \frac{\zeta_{m+1}^{n} - \zeta_{m}^{n}}{\Delta x} = 0 \quad (42)$$

To obtain the final discretized momentum equation for the primitive variable $u_{m+1/2}$, we start with an explicit scheme for the continuity equation (29), which is given by

$$\frac{h_{m}^{n} - h_{m}^{n-1}}{\Delta t} + \frac{\hat{h}_{m+1/2}^{n-1} u_{m+1/2}^{n-1/2} - \hat{h}_{m-1/2}^{n-1} u_{m-1/2}^{n-1/2}}{\Delta x} = 0 \quad (43)$$

Next, we derive an equation by taking the arithmetic average of Eq. (43) in points m and $m+1$, yielding

$$\frac{\overline{h}^{n}_{m+1/2} - \overline{h}^{n-1}_{m+1/2}}{\Delta t} + \frac{\overline{q}^{n^*-1/2}_{m+1} - \overline{q}^{n^*-1/2}_{m}}{\Delta x} = 0 \tag{44}$$

with

$$\overline{q}^{n^*-1/2}_{m} = \frac{1}{2}\left(\hat{h}^{n-1}_{m-1/2} u^{n-1/2}_{m-1/2} + \hat{h}^{n-1}_{m+1/2} u^{n-1/2}_{m+1/2}\right)$$

Multiplying Eq. (44) with $u^{n-1/2}_{m+1/2}$ and subtracting the result from Eq. (42), after which it is divided by $\overline{h}^{n}_{m+1/2}$, gives

$$\begin{aligned} \frac{u^{n+1/2}_{m+1/2} - u^{n-1/2}_{m+1/2}}{\Delta t} &+ \frac{1}{\overline{h}^{n}_{m+1/2}}\left(\frac{\overline{q}^{n-1/2}_{m+1}\hat{u}^{n-1/2}_{m+1} - \overline{q}^{n-1/2}_{m}\hat{u}^{n-1/2}_{m}}{\Delta x} - u^{n-1/2}_{m+1/2}\frac{\overline{q}^{n^*-1/2}_{m+1} - \overline{q}^{n^*-1/2}_{m}}{\Delta x}\right) \\ &+ g\frac{\zeta^{n}_{m+1} - \zeta^{n}_{m}}{\Delta x} = 0 \end{aligned} \tag{45}$$

After the momentum equation (45) is solved, the continuity equation is then solved, which is given by (cf. Eq. (43))

$$\frac{\zeta^{n+1}_{m} - \zeta^{n}_{m}}{\Delta t} + \frac{\hat{h}^{n}_{m+1/2} u^{n+1/2}_{m+1/2} - \hat{h}^{n}_{m-1/2} u^{n+1/2}_{m-1/2}}{\Delta x} = 0 \tag{46}$$

Like the first variant, this scheme preserves non-negativity of the water depth under the CFL condition (38) and remains stable, if

$$\frac{\left[\mid u^{n-1/2}_{m+1/2} \mid + \sqrt{g\hat{h}^{n}_{m+1/2}}\right]\Delta t}{\Delta x} \leq 1$$

In addition, assuming a uniform bathymetry, Eq. (45) conserves momentum per unit length $\overline{h}^{n-1}_{m+1/2} u^{n-1/2}_{m+1/2}$ over time (cf. Eq. (42)). Notice that variants I and III are mathematically equivalent, although they differ in the order of the solution with respect to time stepping.

Concerning the temporal order of accuracy, all three variants are second order accurate in time in the absence of the advection term by virtue of staggering in time. To obtain second order accuracy in both space and time, a predictor-corrector technique is adopted. In the predictor step, the momentum equation (39), (45) or (41) is solved to determine the provisional flow velocities $u^{*}_{m+1/2}$ or momentum values $q^{*}_{m+1/2}$, respectively. In the corrector step, these values are corrected by means of a second order upwind scheme in a deferred correction fashion, while marching in time using the MacCormack approach to achieve second order accuracy in time. See [34] for further details. The accuracy test of this approach will be discussed in Section 6.2.

6. Numerical experiments

6.1. Methods to be assessed

A number of numerical methods for the solution of the depth-integrated shallow water equations has been discussed in the previous sections. In this section, we present three staggered schemes, which in turn

will be assessed in light of the numerical accuracy, stability, robustness and conservation properties. In essence, they are distinguished by the use of dependent variables which are either primitive or flux variables.

Scheme I – `Stagg (ζ,u)`

The first staggered scheme is the third variant of time integration schemes as outlined in Section 5 and is given by Eqs. (45) and (46), augmented with Eqs. (21), (23) and (24). This method employs the primitive variables ζ and u. A key feature of this approach is that the depth-averaged velocity u is transported by the mass flux q, which is computed with Eqs. (20) and (21). Another key aspect is the preservation of non-negativity of the water depth based on condition (38). The method satisfies the Rankine-Hugoniot jump relations (19) and (27), implying continuity of the mass flux and momentum flux across discontinuities, respectively. Furthermore, the scheme is well-balanced, i.e. it preserves exactly the balance between the pressure flux and the bed slope term, so that artificial flows are excluded when quiescent still-water conditions are considered. This first scheme is denoted as `Stagg (ζ,u)`. Note that this approach is implemented in, e.g. SWASH [34]. Also note that this scheme is similar to the one described in [27].

Scheme II – `Stagg U (h,q)`

The second staggered scheme consists of Eqs. (37) and (41) combined with Eqs. (31) and (32). This is also the second variant of time integration schemes presented in Section 5. This scheme uses the water depth h and the depth-integrated velocity q (or momentum per unit length) as the resolved variables. The depth-averaged velocity u is obtained by means of the 'upwind' approach, i.e. Eq. (34). We denote this scheme as `Stagg U (h,q)`. Like the first scheme, this scheme preserves steady-state flows at rest. However, the method does not comply with the jump condition (27), so that it allows to produce odd-even oscillations (viz. Eq. (36)). In addition, the scheme can not ensure non-negativity of the water depth, since a condition like Eq. (38) can not be deduced from this scheme.

Scheme III – `Stagg C (h,q)`

The third staggered scheme is similar to the second one, except the depth-averaged velocity u is estimated via the 'central' approach, i.e. Eq. (33). This scheme is designated as `Stagg C (h,q)`.

6.2. Convergence test

To test the actual order of accuracy of the discussed schemes we will employ the method of manufactured solutions [39]. We consider a progressive wave in a one-dimensional domain of the following form

$$\zeta(x,t) = a_0 \cos\left(2\pi\left[\frac{x}{L} - \frac{t}{T}\right]\right)$$

with a_0, L and T the wave amplitude, length and period, respectively. The bed is uniform. To satisfy continuity equation (14), the mass flux is then given by $q(x,t) = c_0\zeta(x,t)$ with $c_0 = \sqrt{gd}$ the wave speed. Next, this manufactured solution is substituted into momentum equation (15) or (17) yielding non-zero terms, which can be added to the momentum equation. These terms act as forcing terms for preventing the progressive wave from being deformed by nonlinearity. Also, the generation of higher harmonics is precluded. In order to test all terms of the discretized equations, including momentum advection, the amplitude of the chosen solution was set to $a_0 = 0.5d$. The boundary condition at $x = 0$ was $q(t) = a_0 c_0 \cos(2\pi t/T)$ and a zero velocity was applied at $x = 10L$. This boundary location is sufficiently moved away from the domain of interest so as to not to introduce reflection errors in the solution. Both ζ and u were initially set to zero.

A grid refinement study was conducted to assess the convergence properties of the three discussed schemes. For this purpose second order central differences were implemented for the approximation of momentum advection by means of the deferred correction approach [35]. Furthermore, for the computation of $h_{m+1/2}$ the aritmethic average was employed , i.e. $h_{m+1/2} \approx \overline{h}_{m+1/2}$, viz. Eq. (25), instead of Eq. (21). As a consequence, schemes `Stagg U (h,q)` and `Stagg C (h,q)` are identical. Computational grids consisting of 10, 20, 40 and 80 grid cells per wave length were used. In order to keep the Courant number $c_0\Delta t/\Delta x$ constant, the time step Δt was reduced for each grid refinement. A Courant number of 0.2 was chosen, so that 50, 100, 200 and 400 time steps per wave period were employed, respectively.

The root-mean-square errors for $\zeta(x,t)$ and $u(x,t)$ were monitored after five wave periods in a part of the domain, namely $0 \leq x \leq 5L$. The results are displayed in Figure 2. The observed error is a combination

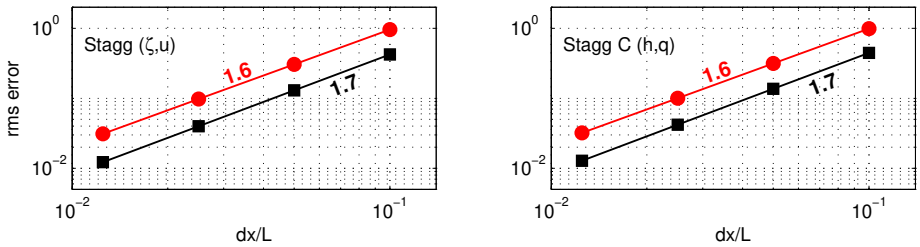

Figure 2: Root-mean-square error in water level ζ (in m; black squares) and in velocity u (in m/s; red dots) at $t = 5T$ as function of grid size obtained with different schemes. The numbers in the plots indicate the rate of convergence.

of spatial and temporal contributions obtained on different grids and time steps. Given the use of relatively

coarse grids, the rate of convergence of schemes `Stagg (ζ,u)` and `Stagg C (h,q)` is inclined to second order with respect to Δx (and to Δt) for both ζ and u.

6.3. Idealized test cases

In this section we present three idealized test cases with the objective of assessing the capabilities and limitations of each of the methods described in Section 6.1. In particular, we will address the following:

- the continuity of mass and momentum flux across a bottom step;
- the avoidance of unwanted effects induced by the checkerboard modes; and
- the accuracy with which either the steady state or unsteady flow solutions are resolved.

The three test cases include (i) expansion in open channel flow; (ii) transition from supercritical to subcritical flow across a bottom step; and (iii) unsteady dam break flow on dry bed.

6.3.1. Subcritical flow over backward facing step

We consider a frictionless channel with a constant width and a jump in the bottom profile as depicted in Figure 3. The length of the channel is 10 km. Upstream of this jump the bed level is 5 m below datum

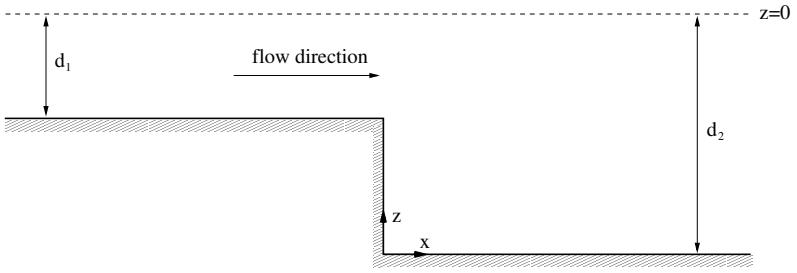

Figure 3: Sketch of expansion flow over a bottom step.

level ($d_1 = 5$ m), and downstream the bed level is 10 m below datum level ($d_2 = 10$ m). Hence, the height of the bottom step is 5 m. In addition, upstream of the jump a discharge of 10 m^2/s is given, whereas downstream a water level of 0 m is imposed. The maximum Froude number for this test is 0.3, so the flow is subcritical everywhere. Based on elementary balance principles in open channel flow [40, 41], the resulted flow experiences an expansion downstream of the jump with a loss in the energy head. Both mass and momentum conservation must hold everywhere. This example is an idealized study of rapidly varied steady flow with an abrupt change in the water depth with which the depth and momentum on either side of the jump is given.

Across the jump we have the following equations

$$u_1 h_1 = u_2 h_2 = 10 \ \mathrm{m}^2\mathrm{s}^{-1}$$

$$u_1^2 h_1 + \frac{1}{2} g \left(h_1 + 5\right)^2 = u_2^2 h_2 + \frac{1}{2} g h_2^2$$

with indices 1 and 2 indicating the locations upstream and downstream of the jump, respectively. Note that the left hand side of the momentum balance includes the hydrostatic pressure against the wall (of the step). Since the downstream water depth is fixed in the test, we will examine the upstream momentum flux obtained with different methods. By means of a rootfinding method its theoretical value is obtained as

$$u_1 q_1 + \frac{1}{2} g h_1^2 = 137.909 \text{ m}^3\text{s}^{-2}$$

To check the continuity of momentum flux across the jump at the discrete level, we consider the following adapted downstream momentum flux

$$u_2 q_2 + \frac{1}{2} g h_2^2 - \frac{5}{2} g \left(h_1 + h_2\right)$$

with the last term representing the topography term. Note that for each method the downstream momentum flux was computed with the indices 1 and 2 corresponding to the consecutive grid points where the actual jump occurred in between.

The mesh width was set to 10 m for all methods, whereas the time step was 0.5 s. This time step was fixed *a priori*, and then left unchanged throughout simulations. It fulfilled the required CFL condition associated with the used schemes (maximum CFL is 0.8).

Initially, both surface elevation and velocity were zero everywhere. The steady state results of the methods are depicted in Figure 4. The first panel illustrates mass conservation: the net mass flux must be zero. The schemes `Stagg (ζ,u)` and `Stagg U (h,q)` appeared to be strictly mass conservative, whereas the `Stagg C (h,q)` method is mass conservative up to machine precision. The second panel demonstrates the continuity of momentum flux across the jump. All methods clearly showed perfect continuity of the momentum flux, implying that they all satisfy jump condition (27). This can be explained by the fact that the gradient of the solution is zero everywhere except at the bottom step, so that the set of finite difference equations automatically reduces to the algebraic expressions (19) and (27). Schemes `Stagg U (h,q)` and `Stagg C (h,q)` underestimated the upstream momentum flux, whereas this flux as computed by `Stagg (ζ,u)` is precisely 137.909 m^3s^{-2}.

Although all discussed schemes comply with the Rankine-Hugoniot relations in the jump region, still the overall numerical solution may not be correct. As pointed out by, e.g. Stelling and Duinmeijer [24], Bernetti et al. [42] and Murillo and Garcia-Navarro [43], the numerical evaluation of the hydrostatic force exerted by the bottom step on the fluid is responsible for this. For instance, Bernetti et al. [42] derive the jump conditions for mass and momentum whereby the total energy across the discontinuity must be dissipated correctly (i.e. the entropy condition is fulfilled). In this way, non-physical solutions are excluded.

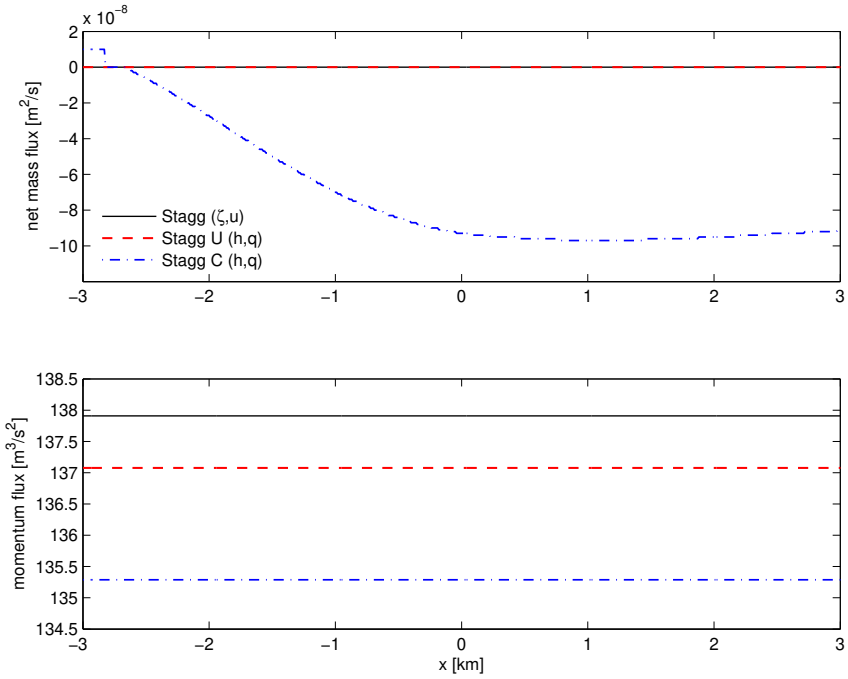

Figure 4: Computed net mass flux (upper panel) and momentum flux (lower panel) along the channel for the expansion flow with a jump in the bed. The location of this jump is $x = 0$.

Let us now return to the expansion flow test. We calculate the downstream momentum flux using the jump conditions of Bernetti et al. [42], as follows

$$u_2 q_2 + \frac{1}{2} g h_2^2 - \frac{1}{2} g \left[h_1 + (\zeta_1 + d_2) \right] (d_2 - d_1) = 137.909 \text{ m}^3\text{s}^{-2}$$

with the indices 1 and 2 corresponding to the first and last grid point of the computational domain, respectively. The third term on the left hand side is the actual horizontal force imposed by the step with height $d_2 - d_1 = 5$ m on the fluid. Table 1 presents a comparison among different schemes with respect to upstream and downstream momentum flux. Only scheme `Stagg (ζ,u)` is perfectly momentum flux conservative, whereas other schemes are not. The explanation for this finding is related to the difference between

Table 1: Comparison of upstream and downstream momentum flux between the discussed schemes for the expansion flow.

scheme	upstream momentum flux (m^3s^{-2})	downstream momentum flux (m^3s^{-2})
`Stagg (ζ,u)`	137.909	137.909
`Stagg U (h,q)`	137.077	138.842
`Stagg C (h,q)`	135.288	140.866

Eq. (36) and Eq. (27), in particular the advection part, owing to the erroneous interpretation of u as the transport velocity. This difference becomes relevant at the shock.

In light of the foregoing, it is expected that scheme `Stagg (ζ,u)` computes the energy dissipation correctly. Now we look at the energy head loss across the shock. A part of the kinetic energy is transformed to potential energy and to energy loss due to expansion. At the discrete level, however, the amount of artificial viscosity induced by a scheme controls the actual amount of loss. Because of continuity, the decrease in the kinetic part of the energy head across the jump is fixed. This implies that the increase in the piezometric head after the expansion is determined solely by the level of artificial dissipation.

The loss in energy head due to expansion can be computed theoretically according to the Borda-Carnot equation [40]

$$\Delta H = \frac{(u_1 - u_2)^2}{2g} = 5.55 \text{ cm}$$

where ΔH is the energy head loss, and the indices 1 and 2 symbolize the location before the flow expansion and after the flow separation, respectively. For each scheme the head loss is computed as follows

$$\Delta H = \zeta_1 - \zeta_2 + \frac{u_1^2 - u_2^2}{2g}$$

of which the results are presented in Table 2. Furthermore, for each scheme the decrease in the kinetic part and the increase in the potential part of the energy head are displayed as well. As expected, scheme

Table 2: Comparison of decrease in kinetic part of energy head, increase in potential part of energy head, and head loss between the discussed schemes for the expansion flow.

scheme	$\Delta\frac{u^2}{2g}$ (cm)	$\Delta\zeta$ (cm)	ΔH (cm)
`Stagg (ζ,u)`	−16.18	10.69	5.49
`Stagg U (h,q)`	−16.36	12.60	3.76
`Stagg C (h,q)`	−16.72	16.72	0.00

`Stagg (ζ,u)` is the most accurate one, i.e. it produces virtually the right amount of energy dissipation. Obviously, this amount is larger than that of scheme `Stagg U (h,q)`, as evidenced by the smaller head loss or higher potential energy. Scheme `Stagg C (h,q)` is seemingly energy head conservative, by which the entropy is likely decreased.

6.3.2. Flow transition over a submerged bottom step

In this example we study the propagation of simple waves (shock and rarefaction waves) and flow transition across a bottom step in a one-dimensional, horizontal, frictionless channel. We consider this channel with a length of 20 m and a step of 1 m in the middle of the channel as depicted in Figure 5. This step

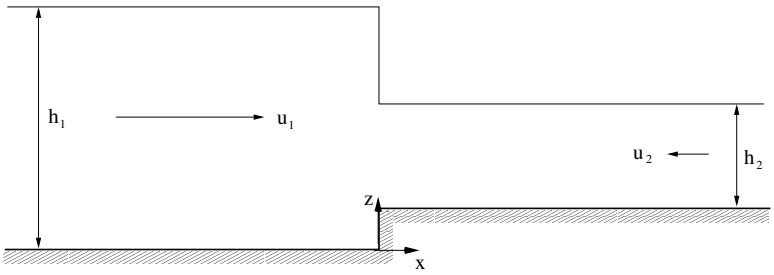

Figure 5: Schematic view of flow transition across a bottom step with initial conditions.

imposes a horizontal thrust on the flow as described by the hydrostatic pressure integrated over the step height [42].

The initial conditions exhibited a discontinuity in the middle of the channel as well (see Figure 5): upstream of the step the water level and flow velocity were 4 m and 15.5 m/s, whereas downstream they were 2 m and -1.55 m/s, respectively. At the left boundary, a water level of 4 m was imposed, whereas at the right boundary a velocity of -1.55 m/s was given. These conditions do not result in a flow acceleration across the bottom step. We compare the model results to the exact solution obtained by solving the associated Riemann problem as outlined in Section 6.2.5 of Alcrudo and Benkhaldoun [44] (their Fig. 19).

The aim of this test case is to investigate the effect of grid spacing on the accuracy of the numerical solution obtained with the discussed methods. For this purpose the simulations were made with grid sizes of 0.05 m, 0.1 m and 0.2 m, and a relatively small but fixed time step of 0.001 s. This time step was chosen as to minimize temporal discretization error. The corresponding Courant numbers based on the upstream water depth and velocity are 0.44, 0.22 and 0.11, respectively. The exception is scheme `Stagg C (h,q)` for which an extremely small time step of 10^{-6} s was chosen to maintain a stable solution.

The results obtained at the finest grid and $t = 0.5$ s is presented in Figure 6. Obviously, scheme `Stagg C (h,q)` was not able to produce a proper solution. The other two schemes resolved the transition from supercritical to subcritical flow and the two shocks correctly [44]. Especially the first order scheme `Stagg (ζ,u)` is superior. In contrast, scheme `Stagg U (h,q)` failed to remove spurious oscillations near second wave front as it does not obey the Rankine-Hugoniot jump condition for momentum (viz. Eq. (36)). Similar observations can be made with respect to coarser grids; see Figures 7 and 8.

The first order scheme `Stagg (ζ,u)` yields a more smooth and less accurate solution on the coarsest grid ($\Delta x = 0.2$ m) compared to the finest one ($\Delta x = 0.05$ m). To increase the spatial accuracy of `Stagg (ζ,u)`, a second order deferred correction to the first order upwind scheme for the momentum advection is introduced, warranting the stability of the whole scheme and the validity of the Rankine-Hugoniot jump relation (27). This correction concerns a second order upwind extrapolation augmented with a slope limiter to avoid unwanted oscillations. For this test, the MUSCL limiter [33, 45] is employed. Further details on this

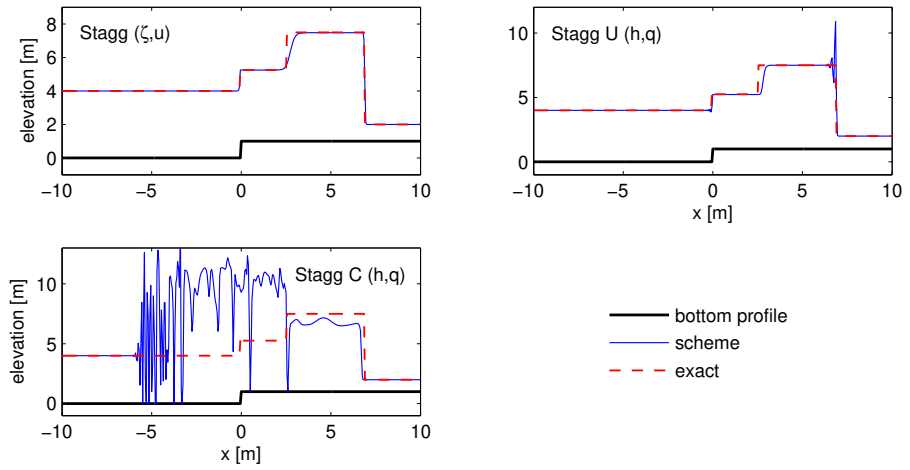

Figure 6: Comparison of surface elevations at $t = 0.5$ s for the flow over a step obtained with different schemes with $\Delta x = 0.05$ m and analytical solution.

approach can be found in [34]. The result is depicted in Figure 9 demonstrating the superiority of the higher order scheme to its lower order counterpart for high-fidelity coarse grid solutions.

6.3.3. Dam break on a dry bed

We consider an unsteady flow with propagation of a dam break wave in a dry horizontal frictionless channel. Initially, the surge front is a sudden discontinuity that involves rapid variations of water depth and flow velocity. It is treated as a Riemann problem for which the exact solution is available [14]. This test case has a distinct feature that in the transition from dry to wet as the bore accelerates, the flow velocity displays a jagged discontinuity whereas the water depth goes smoothly to zero.

The length of the horizontal channel was 100 m, whereas the dam was initially located in the centre of the channel. The ends of the channel were closed (zero discharge). The initial upstream water depth was 1 m, and the downstream water depth was set to 10^{-8} m. This specific case exhibits a transition from subcritical to supercritical flow with a sonic point at the original location of the dam, where $|u| \simeq \sqrt{gh}$.

The grid spacing was 0.05 m for all methods. Next, to obtain a stable solution and non-negative water depths, the time step was set to 0.004 s throughout the simulation for method `Stagg (ζ,u)` (the maximum CFL occurred equals 0.8), whereas scheme `Stagg U (h,q)` remained stable during the simulation with a time step of 0.002 s. We could not achieved a stable solution with method `Stagg C (h,q)`, which will therefore not be discussed in this section.

At time $t = 7$ s after dam failure, the model results of the two stable schemes are depicted in Figure 10. Also shown is the analytical solution. Clearly, the schemes were capable of simulating flow over the dry bed. There is overall agreement between the numerical solutions and analytical one up to $x = 70$ m, displaying a rarefaction wave that propagates upstream the initial discontinuity and a bore that propagates downstream

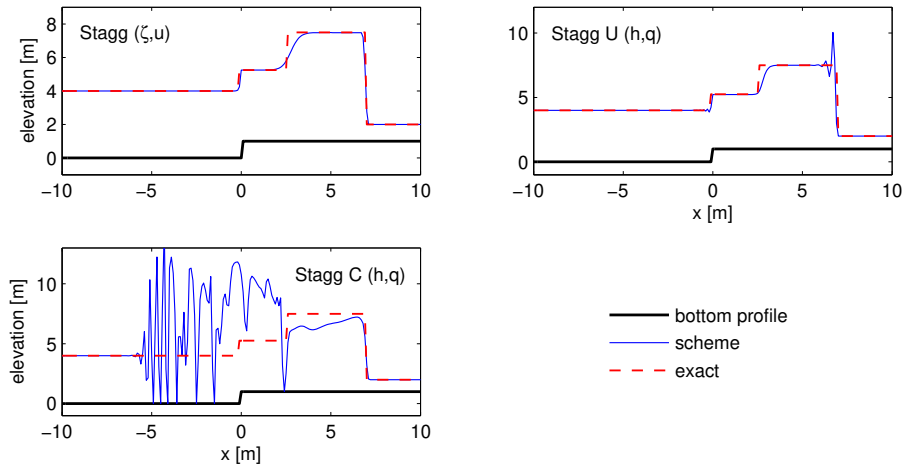

Figure 7: Comparison of surface elevations at $t = 0.5$ s for the flow over a step obtained with different schemes with $\Delta x = 0.1$ m and analytical solution.

over dry bed. This agreement is less satisfactory near the bore front. The presence of spurious oscillations is evident in the results of scheme `Stagg U (h,q)` as depicted in Figure 11, despite the relatively smooth water depth h and depth-integrated velocity q in the transition from dry to wet. The primary cause is a large discontinuity of velocity u in the leading edge of the wave front (see Figure 10), allowing the scheme to produce unphysical oscillations. Indeed, scheme `Stagg U (h,q)` exhibits a checkerboard pattern caused by odd-even decoupling in velocity u (cf. Eq. (36)).

The results of method `Stagg (ζ,u)`, as presented in Figure 11, demonstrate the importance of the conservation of momentum flux $qu + \frac{1}{2}gh^2$ that prevents any spurious oscillations in the solution. In particular, this scheme is very accurate in approaching the wet-to-dry interface, which is attributed to the accuracy with which the momentum flux is conserved (see Section 6.3.1) and the preservation of non-negativity of the water depth. While the height and the speed of the bore are accurately predicted by scheme `Stagg (ζ,u)`, the flow velocity is somewhat underestimated as concluded from Figure 10, although it clearly outperforms scheme `Stagg U (h,q)`.

6.4. Breaking solitary wave running up and down a sloping beach

The discussed schemes have been tested with three idealized cases. This section presents validation of the numerical results with laboratory data from a study concerning solitary wave breaking, runup and rundown on a sloping beach as described in Synolakis [46]. The flume is equipped with a hydraulically smooth bottom which is horizontally flat followed by a plane beach with slope 1:19.85. The data provides, among others, surface profiles under the condition of wave heights of up to 30% of the offshore depth.

Though the nonlinear shallow water equations do not include wave dispersion effects, the measured data enables the assessment of the onset of wave breaking, via steepening of the bore front, and the associated

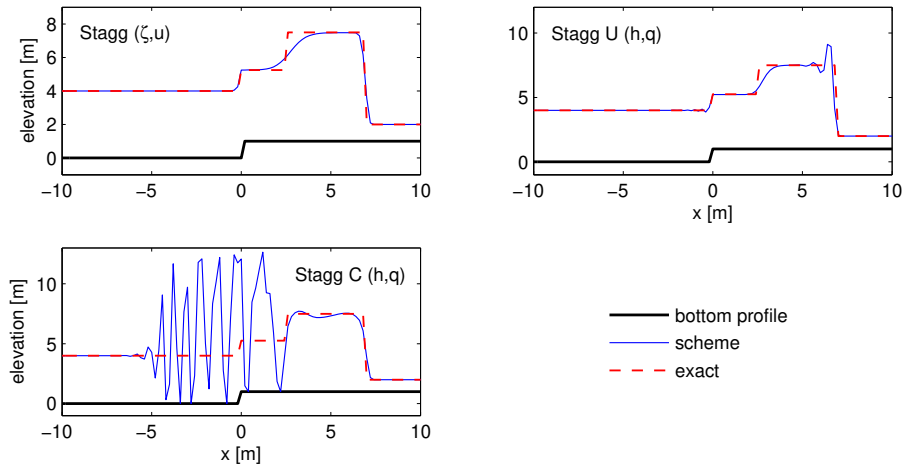

Figure 8: Comparison of surface elevations at $t = 0.5$ s for the flow over a step obtained with different schemes with $\Delta x = 0.2$ m and analytical solution.

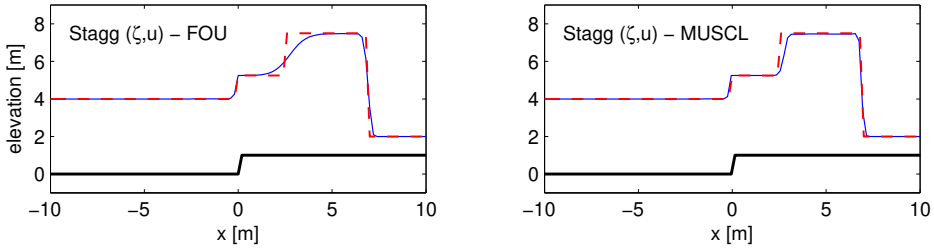

Figure 9: Comparison of surface elevations at $t = 0.5$ s for the flow over a step obtained with scheme `Stagg (ζ,u)` employing first order upwind (left panel) and second order MUSCL extrapolation (right panel) with $\Delta x = 0.2$ m (blue line) and analytical solution (red dashed line). The black line represents the bottom topography.

energy losses, the wave runup on the dry bed, and the formation of hydraulic jump while the wave retreats due to gravity. These processes are all a consequence of the conservation of mass and momentum fluxes across the discontinuity in the flow [47].

An additional numerical challenge is the wetting and drying processes while waves run up and down on the beach. Especially in the transition from wet to dry during the rundown process, prevention of negative water depths becomes relevant as these depths vanish. Whereas staggered schemes can freeze the mass flux out of a dry cell naturally, colocated schemes require special measures with respect to the computation of the outgoing numerical flux at the cell face between a dry and wet cell, such as the approximate Riemann solvers. For instance, Audusse et al. [7] modify the bed elevation and the water depth at the cell interface, for the purpose of a proper reconstruction of the left and right Riemann states, such that a negative water depth in the dry cell is avoided.

A computational model was set up covering a length of $50d$ with d the still offshore water depth, and a

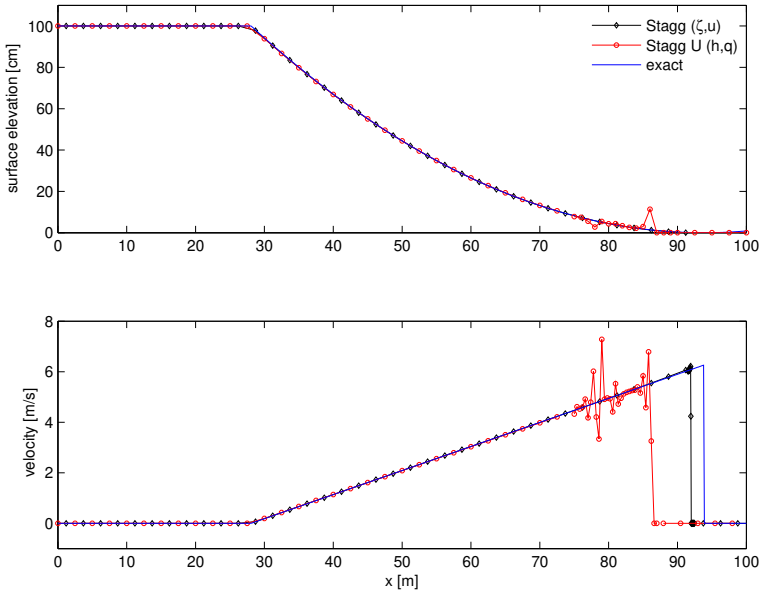

Figure 10: Comparison of free surface (top panel) and velocity (bottom panel) profiles at $t = 7$ s for the dam break wave in a horizontal channel obtained with different schemes and analytical solution.

constant grid size of $\Delta x = 0.125d$. The toe of the slope was located ten times the still water depth from the origin of the domain. Both ends of the domain were closed. Initially, the surface elevation ζ and the flow velocity $\zeta\sqrt{g/d}$ were prescribed based on a solitary wave profile with $H/d = 0.3$ [46]. Here, H denotes the initial wave height of the solitary wave. Furthermore, a fixed time step $\Delta t\sqrt{g/d}$ was chosen so that each method produced a stable solution until the end of the simulation: 0.06, 0.03 and 0.01 for schemes `Stagg (ζ,u)`, `Stagg U (h,q)` and `Stagg C (h,q)`, respectively. The corresponding maximum Courant numbers appeared to be 0.7, 0.4 and 0.3. All the schemes applied to this case were first order accurate in space.

Figure 12 presents the comparison between simulated and measured water levels, normalized by the still

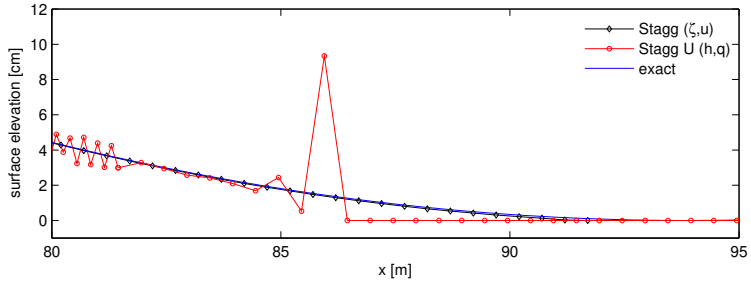

Figure 11: Comparison of bore fronts in the vicinity of transition from dry to wet at $t = 7$ s for the dam break wave in a horizontal channel obtained with different schemes and analytical solution.

offshore water depth, at four different dimensionless times $t\sqrt{g/d}$. The computed surface elevations were obtained with scheme `Stagg (ζ,u)`. The front face of the solitary wave steepens continuously, caused by

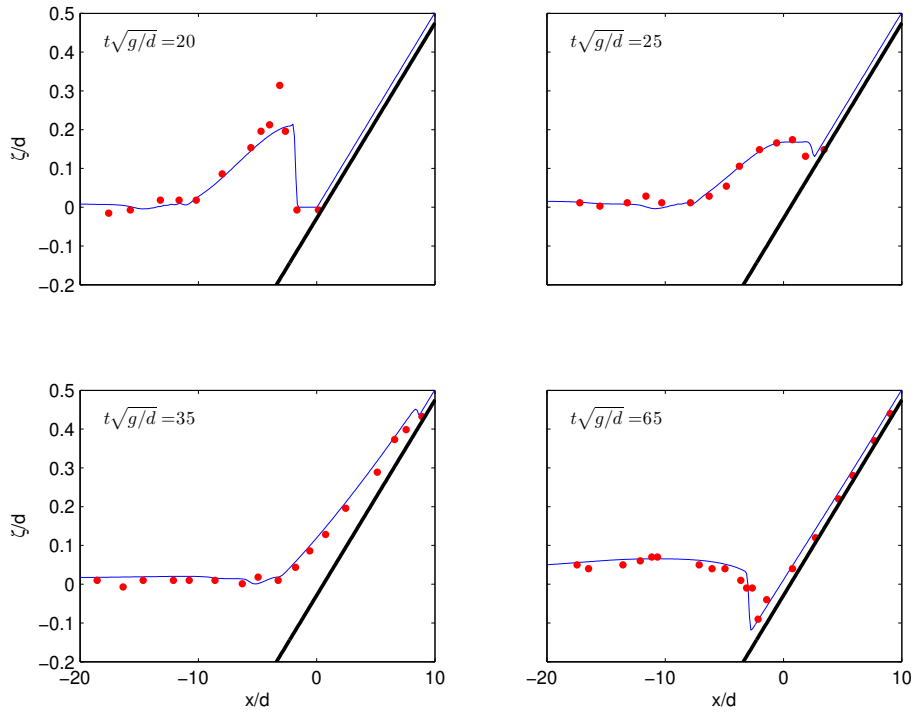

Figure 12: Computed and recorded surface profiles at different times for solitary wave on a sloping beach. Red dots: experimental data of Synolakis [46]; blue thin line: scheme `Stagg (ζ,u)`; black thick line: beach.

nonlinearities, until the front becomes vertical. This steepening must be balanced by the vertical accelerations. The solitary wave in the laboratory test breaks at a time between $t\sqrt{g/d} = 20$ and $t\sqrt{g/d} = 25$ [46]. However, due to the lack of wave dispersivity, scheme `Stagg (ζ,u)` will predict a faster steepening of the bore front and consequently, the simulated bore will break prematurely. The model based on shallow water equations treats broken waves as hydraulic bores. The first panel of Figure 12 displays a well-kept vertical front face that exchanged momentum constantly with the quiescent water ahead and, in turn, the bore collapsed as depicted in the second panel. After breaking, the wave runs up the dry beach at $t\sqrt{g/d} = 25$ to $t\sqrt{g/d} = 45$ [46]. The third panel of Figure 12 demonstrates the ability of method `Stagg (ζ,u)` to reproduce the runup motion accelerated at a proper rate near the shoreline. Rundown starts afterwards while a hydraulic jump is developed. The fourth panel of Figure 12 shows the computed hydraulic jump at the end of the rundown process, which was predicted with fairly good accuracy. From the last two panels, it is obvious that scheme `Stagg (ζ,u)` could cope with the dry to wet transition during runup and the wet to dry transition during rundown.

Results of the other schemes `Stagg U (h,q)` and `Stagg C (h,q)` are depicted in Figures 13 and 14,

respectively. As seen, the computed results by scheme `Stagg U (h,q)` match the measured data reasonably

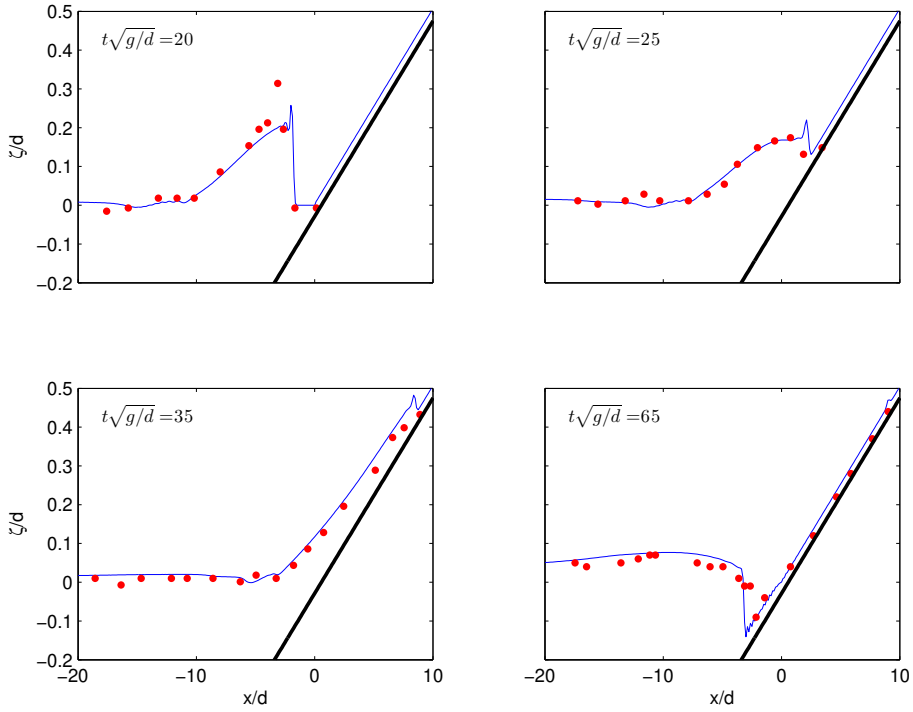

Figure 13: Computed and recorded surface profiles at different times for solitary wave on a sloping beach. Red dots: experimental data of Synolakis [46]; blue thin line: scheme `Stagg U (h,q)`; black thick line: beach.

692

693 well. In contrast, method `Stagg C (h,q)` was not able to properly predict the runup and rundown processes.
694 This is supported by the last two panels of Figure 14. Moreover, both schemes exhibit spurious oscillations.
695 For instance, the fourth panel of both Figures 13 and 14 demonstrates (small) wiggles in the hydraulic
696 jump during the rundown process. Furthermore, it is striking that scheme `Stagg U (h,q)` displays a sharp
697 gradient in the front face of the bore while it runs up the beach (second and third panels of Figure 13).
698 These observations confirm the inability of both methods to preserve the continuity of momentum flux in
699 the discontinuous flow.

700 7. Summary and perspectives

701 The nonlinear shallow water equations may give rise to flow discontinuities that reflect physical phe-
702 nomena like breaking waves in the surf zone, hydraulic jumps and bores. The numerical approach applied
703 is crucial in this matter and should be able to capture such local features in rapidly varied flow with suffi-
704 cient accuracy without losing robustness. Well established methods are the shock capturing finite volume
705 Godunov-type schemes based on approximate Riemann solvers due to their successful performance in the
706 field of gas dynamics. Such schemes require colocation of all the conserved variables.

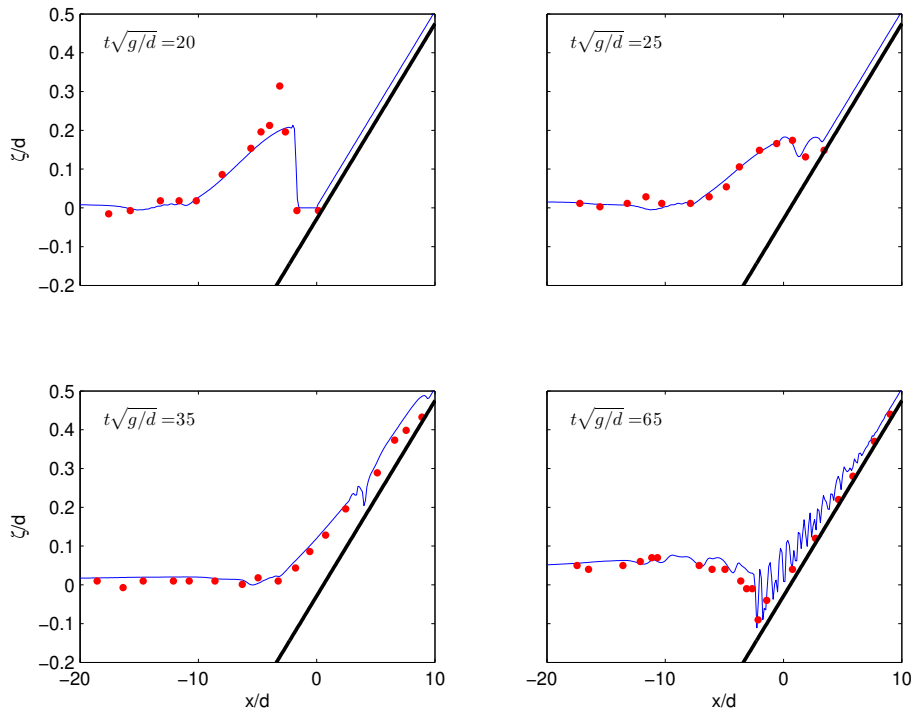

Figure 14: Computed and recorded surface profiles at different times for solitary wave on a sloping beach. Red dots: experimental data of Synolakis [46]; blue thin line: scheme `Stagg C (h,q)`; black thick line: beach.

Another class of numerical methods for solving nonlinear shallow water equations is related to the staggering of the primitive variables that provides simple and compact grid stencils needed for different equations that are solved together. This promotes accurate and efficient discretization of the governing equations. Staggered schemes are usually applied to gradually varied shallow water flows. However, as demonstrated in this paper, such schemes are also suitable for rapidly varied flows provided that the Rankine-Hugoniot jump relations for mass flux and momentum flux are fulfilled at the discrete level. Although these relations are utilized in gas dynamics to identify shock waves and to compute their speed, they can also be employed as jump conditions that must hold across any discontinuities, including hydraulic jumps and bores. Owing to the jump conditions, a two-point upwind discretization must be applied to the advection of momentum, which also generates numerical dissipation needed to avoid oscillations near discontinuities.

One of the main objectives of this study was to assess the performance of three staggered schemes, employing different sets of dependent variables, for the solution of the depth-integrated shallow water equations in one-dimensional domain. Three idealized 1D tests were selected to verify the accuracy and robustness of the discussed schemes. Furthermore, the three schemes were also applied to reproduce a laboratory test of Synolakis [46] concerning breaking, runup and rundown of a solitary wave on a sloping beach. The numerical results were compared with analytical solutions and laboratory measurements.

The discussed schemes make use of a staggered grid layout for the two dependent variables in both space and time: the water levels ζ or water depths h at cell centres and the depth-averaged or depth-integrated velocities at cell faces, u and q, respectively, while the elevation is evaluated before or after the flow speed within one time step. With the exception of the advection term, the remaining terms of the continuity and momentum equations are approximated by means of second order central differences. Due to staggering in time the temporal accuracy of these terms is second order as well. To achieve second order accuracy in both time and space with respect to the advection term, a predictor-corrector technique of the MacCormack type combined with a deferred correction approach [34] can be applied. Convergence tests confirm that the order of spatial and temporal accuracy tends to exhibit second order behaviour, if central differences are applied.

The employed staggered schemes differ from one another in terms of the interpretation of the transport velocity related to the upwind discretization of the advection term: either the mass flux or the flow velocity. The associated momentum to be transported is the depth-averaged velocity (momentum per unit volume) and the depth-integrated velocity (momentum per unit area), respectively. We demonstrated that the former interpretation, i.e. upwinding of the depth-averaged velocity with its direction determined by the mass flux, performs better than the latter interpretation, i.e. upwinding of the depth-integrated velocity with its direction determined by the flow velocity. The key rationale behind this observation is the consistency with the incompressibility constraint while the shallow water equations are elliptic. The first mentioned method use the primitive variables ζ and u and has been designated as `Stagg (ζ,u)` in this study, whereas the latter mentioned method employs flux variables h and q, and is either `Stagg C (h,q)` or `Stagg U (h,q)`.

Another difference between the staggered methods concerns the approximation of the water depth at the cell face to either compute the mass flux or the flow velocity: the first order upwind or second order central approach. As expected, the second option is less robust but formally more accurate than the first option. This second option has been implemented in scheme `Stagg C (h,q)`. In addition, the first option promotes a correct wetting and drying associated with non-negative water depths without distorting the time step, which is confirmed by the numerical tests. In fact, non-negative water depths can be assured if the Courant number based on the flow velocity, being the primitive variable, is below or equal one [24]. This avoids the necessity of involved wetting and drying algorithms. The first option − the upwind approach − has been realized in schemes `Stagg (ζ,u)` and `Stagg U (h,q)`.

The results of the analysis performed and the numerical tests demonstrated that complying with the Rankine-Hugoniot relations for the flux conservation of mass and momentum across a shock or discontinuity is a necessary condition to avoid the odd-even decoupling problem. To be more specific, any attempt to use any data, other than mass flux q, on either side of the discontinuity results in spurious modes, unless the jump conditions for the flux of mass and momentum are invoked. In addition, these jump conditions ensure that solutions are physically realistic (e.g. energy loss across the shock) and provide enhanced numerical stability. This was the second main result of the present work. Only scheme `Stagg (ζ,u)` fully

complies with the jump conditions, produces the correct amount of numerical viscosity at discontinuities, and reveals no evidence of odd-even oscillations in the numerical tests presented in this study. Because of the misinterpretation of the transport velocity and the transported momentum in the upwind discretization of schemes `Stagg U (h,q)` and `Stagg C (h,q)`, strict fulfillment of the jump conditions can not be met, so that these schemes suffer from odd-even oscillations as confirmed by the tests. In addition, scheme `Stagg C (h,q)` lacks the robustness of the other schemes, and appears not to be suitable for the simulation of expansion flows and hydraulic jumps.

The discussed schemes were presented and tested in one spatial dimension as their numerical properties could be clearly explained and illustrated in a transparent manner. Furthermore, such schemes may also be applicable for 1D free surface flows in rivers with variable width and depth. A similar approach is described in [48]. We will now briefly discuss extending numerical methods to two spatial dimensions in the finite volume perspective. Structured or unstructured meshes can be used to deal with this issue.

As the concept of mass and momentum conservation is essentially not different for 1D and 2D flow systems, all the findings of the present study naturally carry over to the case of two-dimensional shallow water problems. Much of the rationale of the numerical approximation of shallow water equations in more than one independent variable can be derived as a natural extension of the material presented in this study. Applied to structured grids, this amounts to perform a dimension-by-dimension extension of 1D discretization of the governing equations in both $x-$ and $y-$directions. Unstructured staggered schemes usually adopt the method of Perot [49] that reconstruct a full velocity vector in each cell circumcenter out of the cell face normal velocities. Subsequently, this cell-centred velocity vector is used to compute the full momentum vector at the face center from which a momentum balance in integral form can be derived that leads naturally to expressions suitable for finite volume discretization. They express the fluxes through every edge of the control volume and the discretization can be treated as a local 1D recurrence relation projected in the direction normal to the interface between adjacent cells of either primal or dual grid. In this respect, as in one-dimensional case, we assume that the solution everywhere in the control volume is constant and subsequently, the flux at each edge of the primal/dual cell is based on the 'upwind' value determined by the component of mass flux normal to the edge. It should be noted, however, that the reconstruction by Perot [49] involves averaging of the velocities which are later advected, and this may again lead to odd-even decoupling, if not carefully treated. In conclusion, accurate and robust 1D schemes are desired for the solution of both one- and two-dimensional problems concerning smooth and discontinuous flows.

Based on the obtained results of the numerical experiments in this study, it can be concluded that 1D scheme `Stagg (ζ,u)` is the most accurate and robust scheme. As has been said, the extension of this recommended scheme to two dimensions is conceptually simple. The favorable properties of the 1D scheme are expected to be transferred to the resulting 2D method. Examples of the application of 1D scheme `Stagg (ζ,u)` for 2D modelling of large-scale shallow water flows on structured and unstructured staggered

meshes can be found in [22–24, 26]. Additionally, it has been successfully used for numerous applications in the simulation of breaking infragravity and short waves on sloping beaches; see, e.g. [50]. All these references demonstrated the accuracy and robustness of the 2D method, emanated from the 1D scheme `Stagg (ζ,u)`, for the simulation of both gradually and rapidly varied shallow water flows.

Acknowledgements

The author would like to thank the anonymous reviewers for their constructive remarks and valuable suggestions which helped to improve the presentation.

References

[1] J. J. Stoker, Water Waves: The Mathematical Theory with Applications, Interscience Publishers, New York, 1957.

[2] P. L. Roe, Approximate Riemann solvers, parameter vectors and difference schemes, J. Comput. Phys. 43 (1981) 357–372.

[3] A. Harten, P. D. Lax, B. Van Leer, On upstream differencing and Godunov-type schemes for hyperbolic conservation laws, SIAM Rev. 25 (1983) 35–61.

[4] R. J. LeVeque, Finite Volume Methods for Hyperbolic Problems, Cambridge University Press, Cambridge, 2004.

[5] E. F. Toro, Riemann Solvers and Numerical Methods for Fluid Dynamics: A Practical Introduction (3rd ed.), Springer-Verlag, Berlin, 2009.

[6] A. Kurganov, D. Levy, Central-upwind schemes for the Saint-Venant system, M2AN Math. Model. Numer. Anal. 36 (2002) 397–425.

[7] E. Audusse, F. Bouchut, M.-O. Bristeau, R. Klein, B. Perthame, A fast and stable well-balanced scheme with hydrostatic reconstruction for shallow water flows, SIAM J. Sci. Comput. 25 (2004) 2050–2065.

[8] U. S. Fjordholm, S. Mishra, E. Tadmor, Well-balanced and energy stable schemes for the shallow water equations with discontinuous topography, J. Comput. Phys. 230 (2011) 5587–5609.

[9] P. Glaister, Approximate Riemann solutions of the shallow-water equations, J. Hydraul. Res. 26 (1988) 293–306.

[10] A. Bermudez, M. E. Vazquez, Upwind methods for hyperbolic conservation laws with source terms, Comp. Fluids 23 (1994) 1049–1071.

[11] P. Garcia-Navarro, M. E. Vazquez-Cendon, On numerical treatment of the source terms in the shallow water equations, Comp. Fluids 29 (2000) 951–979.

[12] J. G. Zhou, D. M. Causon, C. G. Mingham, D. M. Ingram, The surface gradient method for the treatment of source terms in the shallow-water equations, J. Comput. Phys. 168 (2001) 1–25.

[13] B. D. Rogers, A. G. L. Borthwick, P. H. Taylor, Mathematical balancing of flux gradient and source terms prior to using Roe's approximate Riemann solver, J. Comput. Phys. 192 (2003) 422–451.

[14] D. Ambrosi, Approximation of shallow water equations by Roe's Riemann solver, Int. J. Numer. Methods Fluids 20 (1995) 157–168.

[15] J. J. Leendertse, Aspects of a computational model for long-period water-wave propagation, Ph.D. thesis, RM 5294-PR, Rand Corporation, Santa Monica, USA, 1967.

[16] G. S. Stelling, On the construction of computational methods for shallow water flow problems, Ph.D. thesis, Rijkswaterstaat communications no. 35, 1984.

[17] V. Casulli, Semi-implicit finite difference methods for the two-dimensional shallow water equations, J. Comput. Phys. 86 (1990) 56–74.

[18] P. K. Stansby, Semi-implicit finite volume shallow-water flow and solute transport solver with k-ε turbulence model, Int. J. Numer. Methods Fluids 25 (1997) 285–313.

[19] R. A. Falconer, Temperature distributions in tidal flow field, J. Environ. Eng. 110 (1984) 1099–1116.

[20] X. Chen, An efficient finite difference scheme for free-surface flows in narrow rivers and estuaries, Int. J. Numer. Methods Fluids 42 (2003) 233–247.

[21] G. R. Lesser, J. A. Roelvink, J. A. T. M. van Kester, G. S. Stelling, Development and validation of a three-dimensional morphological model, Coast. Eng. 51 (2004) 883–915.

[22] H. Cui, J. D. Pietrzak, G. S. Stelling, A finite volume analogue of the $P_1^{\mathrm{NC}} - P_1$ finite element: with accurate flooding and drying, Ocean Modell. 35 (2010) 16–30.

[23] J. G. Zhou, P. K. Stansby, 2D shallow water model for the hydraulic jump, Int. J. Numer. Methods Fluids 29 (1999) 375–387.

[24] G. S. Stelling, S. P. A. Duinmeijer, A staggered conservative scheme for every Froude number in rapidly varied shallow water flows, Int. J. Numer. Methods Fluids 43 (2003) 1329–1354.

[25] P. A. Madsen, H. J. Simonsen, C.-H. Pan, Numerical simulation of tidal bores and hydraulic jumps, Coast. Eng. 52 (2005) 409–433.

[26] S. C. Kramer, G. S. Stelling, A conservative unstructured scheme for rapidly varied flows, Int. J. Numer. Methods Fluids 58 (2008) 183–212.

[27] D. Doyen, P. H. Gunawan, An explicit staggered finite volume scheme for the shallow water equations, in: J. Fuhrmann (Ed.), Finite Volumes for Complex Applications VII - Methods and Theoretical Aspects, Springer, 227–235, 2014.

[28] F. Alcrudo, P. Garcia-Navarro, A high-resolution Godunov-type scheme in finite volumes for the 2D shallow-water equations, Int. J. Numer. Methods Fluids 16 (1993) 489–505.

[29] D. Liang, B. Lin, R. A. Falconer, Simulation of rapidly varying flow using an efficient TVD-MacCormack scheme, Int. J. Numer. Methods Fluids 53 (2007) 811–826.

[30] B. M. Ginting, A two-dimensional artificial viscosity technique for modelling discontinuity in shallow water flows, Appl. Math. Model. 45 (2017) 653–683.

[31] W. Hansen, Theorie zur errechnung des wasserstandes und der strömungen in randmeeren nebst anwendungen, Tellus 8 (1956) 287–300.

[32] J. D. Anderson Jr., Computational Fluid Dynamics: The Basics with Applications, McGraw Hill, New York, 1995.

[33] C. Hirsch, Numerical Computation of Internal and External Flows, Vol. 2, John Wiley and Sons, Chichester, 1990.

[34] M. Zijlema, G. S. Stelling, P. B. Smit, SWASH: an operational public domain code for simulating wave fields and rapidly varied flows in coastal waters, Coast. Eng. 58 (2011) 992–1012.

[35] P. K. Khosla, S. G. Rubin, A diagonally dominant second-order accurate implicit scheme, Comp. Fluids 2 (1974) 207–209.

[36] Y. Yamazaki, Z. Kowalik, K. F. Cheung, Depth-integrated, non-hydrostatic model for wave breaking and run-up, Int. J. Numer. Methods Fluids 61 (2009) 473–497.

[37] J. G. Zhou, Velocity-depth coupling in shallow-water flows, J. Hydraul. Eng. 121 (1995) 717–724.

[38] M. Zijlema, G. S. Stelling, Further experiences with computing non-hydrostatic free-surface flows involving water waves, Int. J. Numer. Methods Fluids 48 (2005) 169–197.

[39] P. J. Roache, Verification and Validation in Computational Science and Engineering, Hermosa Publishers, Albuquerque, NM, 1998.

[40] H. Chanson, The Hydraulics of Open Channel Flow: An Introduction (2nd ed.), Butterworth-Heinemann, Oxford, 2004.

[41] J. A. Battjes, R. J. Labeur, Unsteady Flow in Open Channels, Cambridge University Press, Cambridge, 2017.

[42] R. Bernetti, V. A. Titarev, E. F. Toro, Exact solution of the Riemann problem for the shallow water equations with discontinuous bottom geometry, J. Comput. Phys. 227 (2008) 3212–3243.

[43] J. Murillo, P. Garcia-Navarro, Weak solutions for partial differential equations with source terms: application to the shallow water equations, J. Comput. Phys. 229 (2010) 4327–4368.

[44] F. Alcrudo, F. Benkhaldoun, Exact solutions to the Riemann problem of the shallow water equations with a bottom step, Comp. Fluids 30 (2001) 643–671.

[45] B. Van Leer, Towards the ultimate conservative difference scheme. V. A second-order sequel to Godunov's method, J. Comput. Phys. 32 (1979) 101–136.

[46] C. E. Synolakis, The runup of solitary waves, J. Fluid Mech. 185 (1987) 523–545.

[47] H. H. Yeh, A. Ghazali, I. Marton, Experimental study of bore run-up, J. Fluid Mech. 206 (1989) 563–578.

[48] N. Goutal, F. Maurel, A finite volume solver for 1D shallow-water equations applied to an actual river, Int. J. Numer. Methods Fluids 38 (2002) 1–19.

[49] B. Perot, Conservation properties of unstructured staggered mesh schemes, J. Comput. Phys. 159 (2000) 58–89.

[50] D. P. Rijnsdorp, B. G. Ruessink, M. Zijlema, Infragravity-wave dynamics in a barred coastal region, a numerical study, J. Geophys. Res. 120 (2015) 4068–4089.